

## Geochemistry of Proterozoic clastic rocks of the Kerur Formation of Kaladgi-Badami Basin, North Karnataka, South India: implications for paleoweathering and provenance

Ariputhiran RAMACHANDRAN<sup>1</sup>, Jayagopal MADHAVARAJU<sup>2,\*</sup>, Sooriamuthu RAMASAMY<sup>3</sup>, Yong IL LEE<sup>4</sup>, Sesha RAO<sup>5</sup>,  
David Lalhmिंगliana CHAWNGTHU<sup>3</sup>, Kasilingam VELMURUGAN<sup>3</sup>

<sup>1</sup>Department of Geology, Anna University, CEG Campus, Guindy, Chennai, India

<sup>2</sup>Northwest Regional Station, Institute of Geology, National Autonomous University of Mexico, Hermosillo, Sonora, Mexico

<sup>3</sup>Department of Geology, School of Earth and Atmospheric Sciences University of Madras, Guindy Campus, Chennai, India

<sup>4</sup>School of Earth and Environmental Sciences, Seoul National University, Seoul, South Korea

<sup>5</sup>Atomic Minerals Directorate for Exploration and Research, Southern Region, Nagarbhavi, Bangalore, India

Received: 04.03.2015 • Accepted/Published Online: 12.11.2015 • Final Version: 08.02.2015

**Abstract:** Major, trace, and rare earth element (REE) studies have been conducted on the Proterozoic clastic rocks of the Kerur Formation of the Kaladgi-Badami Basin, South India, to determine their paleoweathering conditions and provenance characteristics. Geochemically, these sedimentary rocks are classified as quartz arenite, arkose, litharenite, and sublitharenite. The chemical index of alteration values and the A-CN-K diagram suggest that the clastics rocks in this study underwent moderate to intensive weathering. Chondrite-normalized REE patterns with light REE enrichment, flat heavy REE, and a negative Eu anomaly also attribute felsic source-rock to sedimentary rocks of the Kerur Formation. In addition,  $\text{Eu}/\text{Eu}^*$  (~0.77),  $(\text{La}/\text{Lu})_{\text{cn}}$  (~7.65),  $\text{La}/\text{Sc}$  (~5.39),  $\text{Th}/\text{Sc}$  (~3.49),  $\text{La}/\text{Co}$  (~6.79), and  $\text{Cr}/\text{Th}$  (~0.31) ratios support a felsic source for these rock types. Comparing REE patterns and Eu anomalies of the source rocks reveals that the Kerur Formation clastic rocks received a major contribution of sediments from the Dharwar Craton.

**Key words:** Geochemistry, Proterozoic, paleoweathering, provenance, Kerur Formation, Kaladgi-Badami Basin

### 1. Introduction

The geochemistry of clastic sedimentary rocks reflects the tectonic setting of the basin and also provides insights into the chemical environment of deposition (Maynard et al., 1982; Bhatia and Crook, 1986; Roser and Korsch, 1986, 1988; Erickson et al., 1992). Many workers have tried to provide a detailed geochemical analysis to interpret the source rock and depositional environments (Grout, 1925; Degens, 1965; Ernst, 1970; Fralic and Kronberg, 1997; Madhavaraju and Ramasamy, 2001; Armstrong-Altrin et al., 2004, 2013; Ramasamy et al., 2007; Kadir et al., 2013; Göz et al., 2014; Zaid and Gahtani, 2015). Major and trace element geochemistry of sedimentary rocks is considered as a valuable tool to identify the provenance and tectonic setting (Schoenborn and Fedo, 2011; Zhang et al., 2011; Concepcion et al., 2012; Srivastava et al., 2013; Young et al., 2013; Armstrong-Altrin et al., 2014). The trace element contents of sediments and sedimentary rocks have been widely used to investigate sediment provenance (Armstrong-Altrin et al., 2004, 2012; Nagarajan et al.,

2007a, 2007b; Madhavaraju et al., 2010; Moosavirad et al., 2012; Yang et al., 2012; Kùlah et al., 2014; Madhavaraju, 2015) and weathering intensity (Madhavaraju and Ramasamy, 2002; Selvaraj and Chen, 2006; Gupta et al., 2012; Raza et al., 2012), and to understand the depositional environment (Gürel and Kadir, 2010; Jung et al., 2012; Madhavaraju and González-León, 2012; Verma and Armstrong-Altrin, 2013).

In this study, an attempt has been made to ascertain the major, trace, and rare earth elements (REEs) of the sedimentary rocks of the Kerur Formation. Dey et al. (2009) conducted a geochemical study on the sedimentary rocks of the Kaladgi-Badami Basin that mainly focused on the major and trace elements of sandstones to unravel the paleoweathering and provenance signatures. They found that these sandstones showed large variations in weathering history (including chemical index of alteration (CIA) values) and were derived from varied sources; however, they did not properly explain the variations in CIA values or the nature of the source rocks. In this paper,

\* Correspondence: [mj@geologia.unam.mx](mailto:mj@geologia.unam.mx)

we give special attention to the clastic rocks (DNR-58 core samples) of the Kerur Formation of Proterozoic age in an effort to determine the composition of sandstones of the Kerur Formation, evaluate the exact reasons for variations in paleoweathering, and deduce the nature of the source rocks.

**2. Geology and stratigraphy**

The area of the study lies within the well-known Proterozoic Karnataka-Kaladgi Basin (Figure 1), which covers an area of 8000 km<sup>2</sup>. The sediments occur in an east-west trending basin with irregular boundaries and are distributed in the northern districts of Karnataka, principally in the Belgaum, Bijapur, Dharwar, and Gulbarga districts. They are comparatively less disturbed shallow marine sediments, deposited over the eroded basement rocks of gneisses and schists and Archaean granites in the Kaladgi-Badami Basin (after Jayaprakash et al., 1987; Table 1).

The Badami Group overlies both the sediments of the Bagalkot Group and basement granitoids with a distinct angular unconformity and is marked by the presence of a conglomerate in the bottom-most part. The Badami Group includes two formations: the Kerur Formation and

the Katageri Formation. The Kerur Formation consists of three members: the Kendur Conglomerate, the Cave Temple Arenite, and the Halgeri Shale. The Kendur Conglomerate is seen overlying the different rock types, namely granitoids, metasediments, and a few members of the underlying Bagalkot Group, thus representing the presence of a major unconformity prior to its deposition with a gradational contact conglomerate into the Cave Temple Arenites in Badami, where it is well developed, and forms flat-topped barren hillocks with vertical scarps; in other places, it occurs as small mounds and elevated grounds. The Halgeri Shale shows limited exposures and a thickness of less than 4 m; this member is well recognized around Halgeri and Belikhindi. Bottle green to greenish yellow in color, it is friable, silty shale with convolute laminations and is rich in micaceous minerals.

The Katageri Formation is mainly divided into three distinct members: the Belikhindi Arenite, the Halkurki Shale, and the Konkankoppa Limestone. The Belikhindi Arenite is in sharp contact with the underlying Halgeri Shale Member. This unit has a peculiar geomorphic expression, forming smooth hills with a lighter tone and a thin soil cover that supports thorny bushes. The

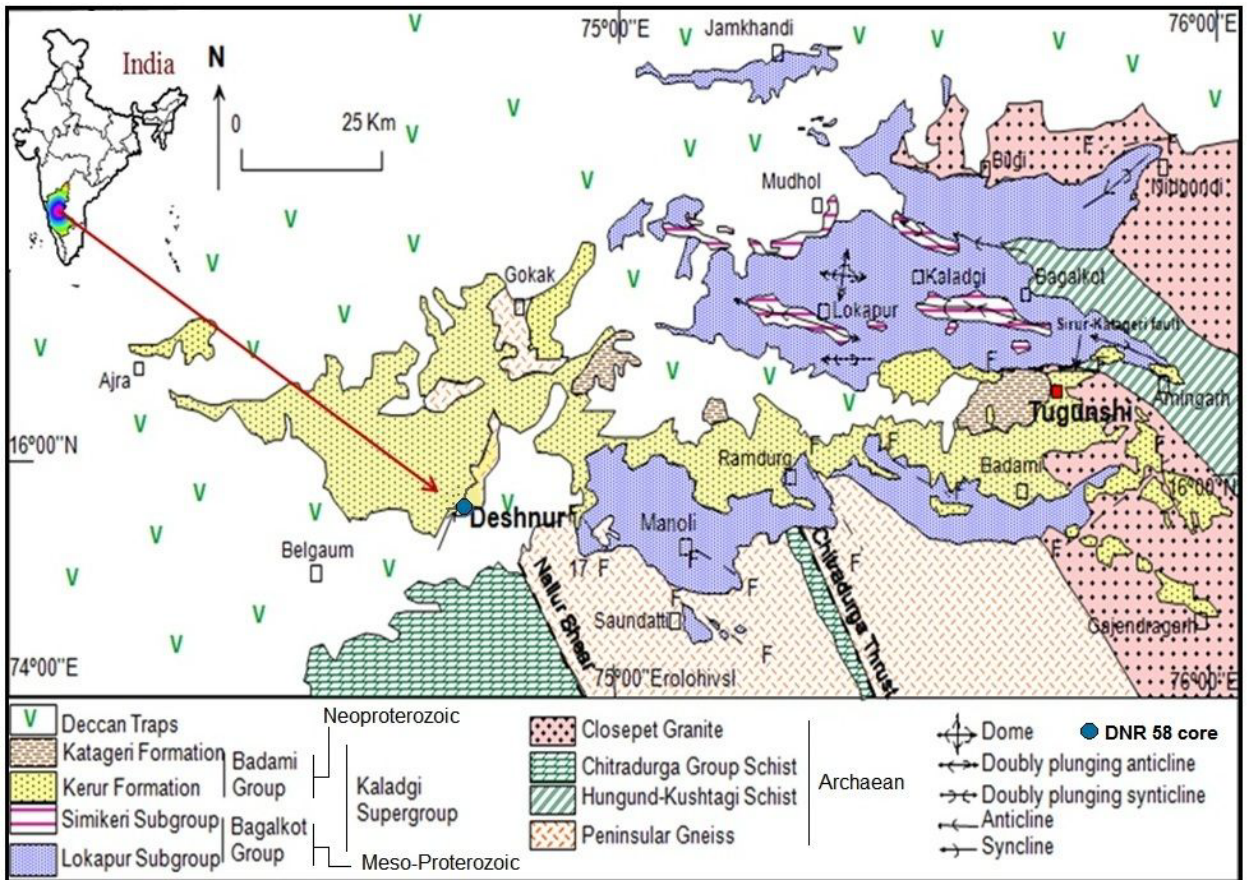


Figure 1. Geological map of the study area (after Jayaprakash et al., 1987; Dey et al., 2009).

**Table 1.** Lithostratigraphy of the Kaladgi-Badami Basin (after Jayaprakash et al., 1987).

Age	Group	Subgroup	Formation	Member	Thickness (m)	
Neoproterozoic	Badami Group		Katageri Formation	Konkankoppa Limestone	85	
				Halkurki Shale	69	
				Belikhindi Arenite	39	
				Kerur Formation	Halgeri Shale	3
				Cave Temple Arenite	89	
				Kendur Conglomerate	3	
Angular unconformity						
Paleo-Mesoproterozoic		Semiri Subgroup	Hoskatti Formation	Mallapur Intrusive Dadanhatti Argillite	7 695	
			Arlikatti Formation	Lakshnhatti Dolomite Keralmatti Hematite Schist Niralkeri Chert-Breccia	87 42 39	
			Kundargi Formation	Govindkoppa Argillite Muchkundi Quartzite Bevinmatti Conglomerate	80 182 15	
	Disconformity					
	Bagalkot Group	Lokapur Subgroup	Yadhalli Formation	Argillite	58	
			Muddapur Formation	Bamanbudnal Dolomite Petlur Limestone Jalikatti Argillite	402 121 43	
			Yendigeri Formation	Naganur Dolomite Chiksellikere Limestone Hebbal Argillite	93 93 166	
			Yargatti Formation	Chitrabhanukot Dolomite Muttalgeri Argillite Mahakut chert-breccia	218 502 133	
			Ramdurg Formation	Manoli Argillite Saundatti Quartzite Salgundi Conglomerate	61 383 31	
	Nonconformity					
Archaean	Granitoids, gneisses, and metasediments					

Halkurki Shale exhibits good exposures around Halkurki with a thickness of approximately 70 m. It is chocolate brown to dark brown in color and is finely laminated to distinctly bedded, with prominent fissility. This unit is in some places interlaminated with fine sandy matter and also bears some carbonates. Warping and local slumping of penecontemporaneous origin and minor faults are commonly observed in this member. The Konkankoppa Limestone shows a gradational contact with the underlying shale; beds around Konkankoppa are flaggy and medium-bedded, suggesting a higher content of insoluble materials.

It is bottle green, cream, buff, and pale gray in color with frequent shale partings, and fine color banding.

### 2.1. Lithology of the Badami Group in the Deshnur area

Type exposures are seen on two sides of the town of Badami, forming a chain of picturesque outcrop that extends from Gajendragad in the east to Gotak in the west. The Badami, as a younger group within the Kaladgi-Badami Basin, is separated by a clearly recognizable angular unconformity between Lower Bagalkot and the overlying Badami rocks.

The Deshnur area represents the western part of the Mesoproterozoic Kaladgi Basin, exposing sediments

of the Badami Group. In the Deshnur area, only the Kerur Formation with its lower two members, the Kendur Conglomerate and the Cave Temple Arenite, are represented. These sediments consist of coarse clastics of arenite and conglomerate, trending east-west with a 10° to 20° dip north, and they rest nonconformably on basement rocks that consist of quartz-chlorite-sericite schist/metabasic rock of the Chitradurga Group. In the Deshnur area, the unconformity surface is obscured by thick soil cover and a thin veneer of Deccan basalt toward the south, which is under soil cover.

## 2.2. Lithology of a DNR-58 core from the Deshnur area

During field studies undertaken from 2009 to 2012, the following three litho-units, with distinct lithological characters, were identified: lower conglomerate, followed by quartz arenite and upper conglomerate, from the bottom up. A thin unit of basal arenite is found only in the bore holes, sandwiched between lower conglomerate and schistose basement rocks. The Atomic Minerals Division (DAE) of the Government of India drilled several boreholes for uranium investigation. We collected samples from a DNR-58 core for geochemical studies (Figure 2) to understand the paleoweathering and provenance of the Kerur Formation.

The total depth of the core is 222.45 m (Figure 3). The basement is chlorite schist overlain by a sedimentary cover: basal arenite, then lower conglomerate followed by quartz arenite. The basement chlorite schist encloses pyrite minerals in dispersed forms. The basement is overlain by basal arenite rock interbedded with conglomerate and several thin bands of shale. The basal arenite is succeeded by lower conglomerate and then by quartz arenite. For the present study, samples were collected from depths of 222.45 to 2 m. All the sample lithologies belong to the Kerur Formation. The basal unit observed in the core section is completely absent in the outcrop sequences. The lower conglomerate unit observed in the DNR-58 core can be correlated to the Kendur Conglomerate Member and the quartz arenite unit belongs to the Cave Temple Arenite Member.

## 3. Materials and methods

Thirty-four samples from the DNR-58 core were selected for geochemical analyses and were subsequently powdered in an agate mortar. Major elements were analyzed for 34 samples using a Siemens SRS-3000 X-ray fluorescence spectrometer with an Rh-anode X-ray tube as a radiation source, at the Institute of Geology, National Autonomous University of Mexico (UNAM), Mexico. One gram of sample was heated to 1000 °C in a porcelain crucible for

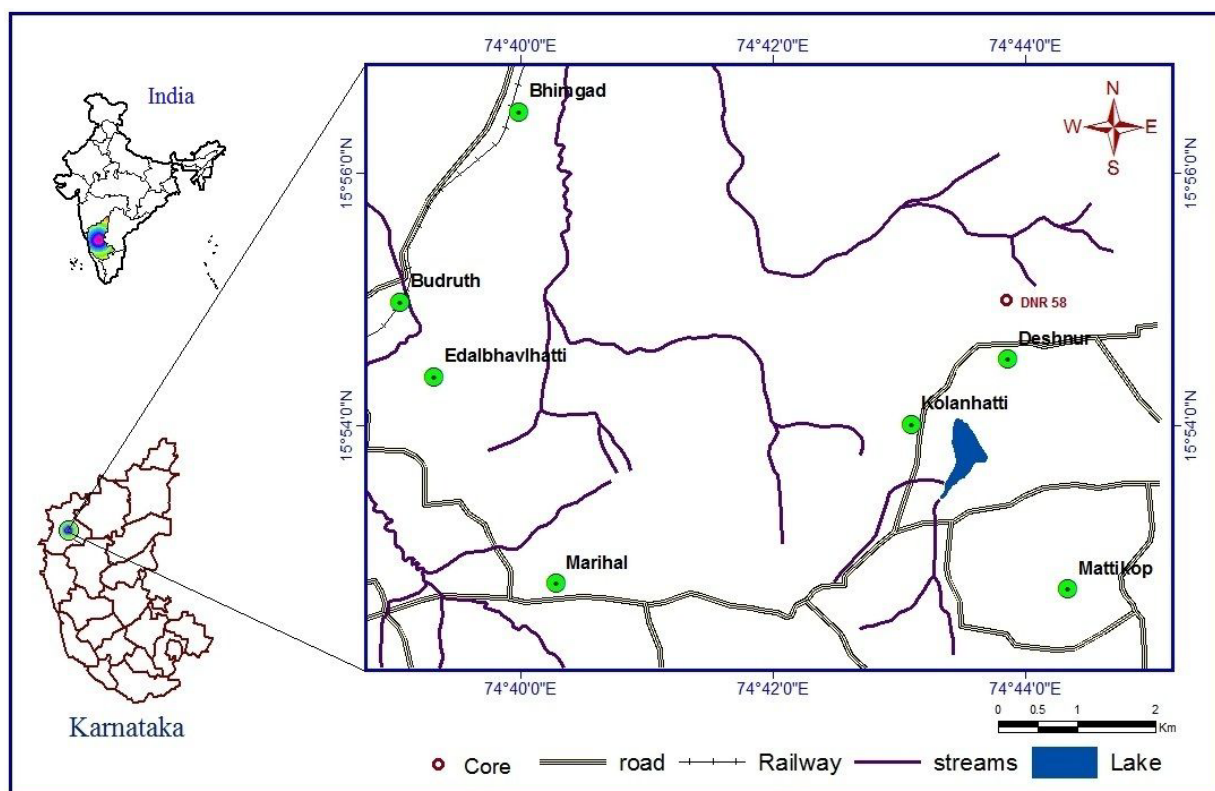


Figure 2. Location map of the study area.

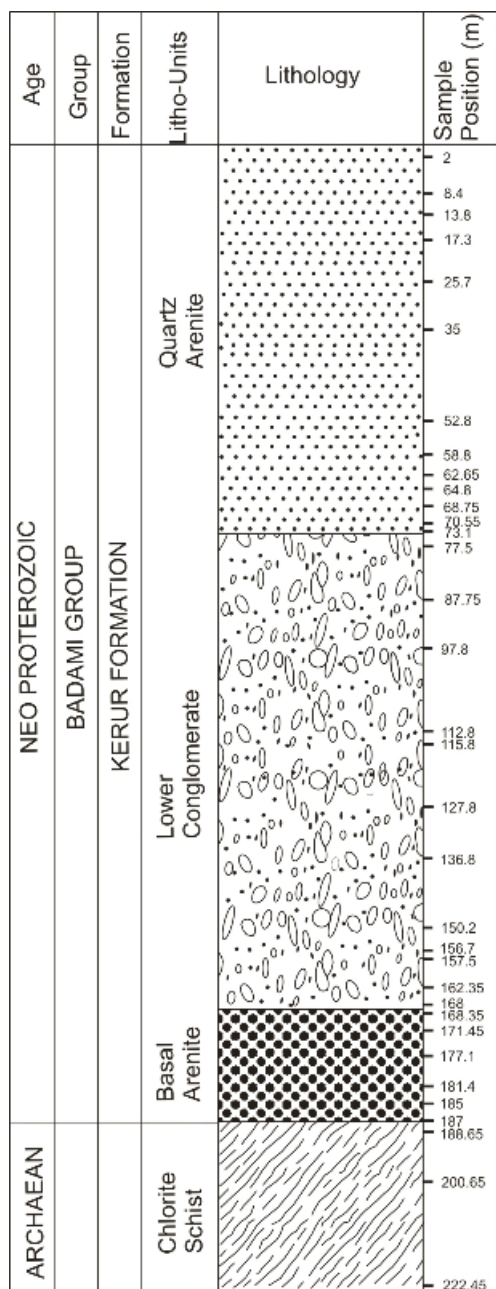


Figure 3. Lithostratigraphic section of the DNR-58 core.

1 h to measure the loss on ignition (LOI). The geochemical standard JGB1 (GSJ) was used to check data quality. Analytical accuracy was better than  $\pm 2\%$  for  $\text{SiO}_2$ ,  $\text{Fe}_2\text{O}_3$ ,  $\text{CaO}$ , and  $\text{TiO}_2$  and better than  $\pm 5\%$  for  $\text{Al}_2\text{O}_3$ ,  $\text{MgO}$ ,  $\text{Na}_2\text{O}$ ,  $\text{K}_2\text{O}$ ,  $\text{MnO}$ , and  $\text{P}_2\text{O}_5$ .

Trace elements and REEs were analyzed for 25 samples using an Agilent 7500ce inductively coupled plasma mass spectrometer (ICP-MS) at the Institute of Geology, UNAM, Mexico. The standard analytical procedures suggested by Eggins et al. (1997) were followed in this study.

Geochemical standards GSR2 and OU8 (Govindaraju, 1994) were used to monitor the analytical reproducibility. The analytical precision errors for Ba, Sc, Y, Sr, Cr, Zn, V, Zr, Nb, Rb, Zn, and Pb were better than  $\pm 5\%$ , whereas the analytical accuracy errors for Cu, Ni, Th, and U were better than  $\pm 10\%$ . The accuracy errors of REEs such as La, Ce, Pr, Nd, Sm, Eu, Dy, Ho, Er, and Yb were better than 5% and those of Gd, Tb, Tm, and Lu were better than  $\pm 10\%$ . Chondrite values (Taylor and McLennan, 1985) were used for REE-normalized diagrams.

## 4. Results

### 4.1. Elemental variations

The major element compositions of the present study are given in Table 2. Using a geochemical classification diagram (Herron, 1988), the different lithologies are classified into litharenite, sublitharenite, subarkose, and quartz arenite (Figure 4). The arenites have a high  $\text{SiO}_2$  concentration ranging from 79.72% to 98.07% (except one basal arenite sample that shows 53.51%). The lower conglomerate and basal arenite samples are higher in  $\text{Al}_2\text{O}_3$  content (2.41% to 7.08%, 2.61% to 22.2%, respectively) than the quartz arenite (0.70% to 4.58%). The  $\text{Fe}_2\text{O}_3$  content has a wide range in quartz arenite, lower conglomerate, and basal arenite (Table 2). The  $\text{K}_2\text{O}/\text{Al}_2\text{O}_3$  ratios of terrigenous sedimentary rocks can be used as an indicator of the original composition of ancient sediments because the  $\text{K}_2\text{O}/\text{Al}_2\text{O}_3$  ratios for clay minerals and feldspars are different.  $\text{K}_2\text{O}/\text{Al}_2\text{O}_3$  ratios for clay minerals range from 0.0 to 0.3 and for feldspars range between 0.3 and 0.9 (Cox and Lowe, 1995a). In the present study, the  $\text{K}_2\text{O}/\text{Al}_2\text{O}_3$  ratio varies as follows: basal arenite ( $0.61 \pm 0.33$ ,  $n = 6$ ), lower conglomerate ( $0.70 \pm 0.11$ ,  $n = 12$ ), and quartz arenite ( $0.22 \pm 0.03$ ,  $n = 13$ ), which suggests that basal arenite and lower conglomerate contain considerable amounts of feldspar grains.  $\text{SiO}_2$  shows significant negative correlations with  $\text{Al}_2\text{O}_3$  (Figure 5), suggesting that most of the  $\text{SiO}_2$  is present as quartz grains.

The concentrations of trace elements and their ratios are given in Table 3. The quartz arenite samples are lower in large ion lithophile elements (LILEs: Rb, Cs, Ba, and Sr) than in lower conglomerate and basal arenite (Figure 6; Table 3). In comparison with upper continental crust (UCC), the quartz arenites are depleted in Co, Sr, Rb, Ba, and Nb. Sr is depleted in both lower conglomerate and basal arenite samples. Most of the transition trace elements (TTEs: Co, Ni, V, and Cr) and high field strength elements (HFSEs: Zr, Y, Nb, and Hf) show wide variations compared to UCC (Figure 6).  $\text{Al}_2\text{O}_3$  and  $\text{K}_2\text{O}$  are positively correlated with Rb, Ba, and Sr in the lower conglomerate ( $\text{Al}_2\text{O}_3$ :  $r = 0.88$ ,  $r = 0.73$ ,  $r = 0.74$ , respectively;  $\text{K}_2\text{O}$ :  $r = 0.98$ ,  $r = 0.94$ ,  $r = 0.96$ , respectively) and basal arenite ( $\text{Al}_2\text{O}_3$ :  $r = 0.99$ ,  $r = 0.96$ ,  $r = 0.91$ , respectively;  $\text{K}_2\text{O}$ :  $r = 0.99$ ,  $r = 0.98$ ,  $r = 0.95$ , respectively), suggesting that these trace elements are

**Table 2.** Major oxides variations (wt%) in the clastic rocks of the Kerur Formation.

Lithology	Quartz arenite															Lower conglomerate					
	2.0	8.4	13.8	17.3	25.7	35	52.8	58.8	62.65	64.8	68.75	70.55	73.1	77.5	87.75	97.8	112.8				
Depth (m)	97.78	97.56	97.01	93.57	98.07	87.2	95.65	97.34	97.11	94.77	95.96	98.05	96.25	95.92	91.12	94.04	91.96				
SiO <sub>2</sub>	1.03	0.98	1.61	2.86	0.86	4.58	2.49	1.32	1.27	2.91	2.41	0.7	2.08	2.41	4.59	3.71	3.14				
Al <sub>2</sub> O <sub>3</sub>	0.23	0.58	0.4	1.4	0.19	5.31	0.31	0.51	0.25	0.35	0.27	0.58	0.22	0.21	1.31	0.34	2.13				
Fe <sub>2</sub> O <sub>3</sub>	0.02	0.01	0.01	0.03	0.01	0.01	0.01	0.01	0.01	0.01	0.01	0.02	0.01	0.01	0.02	0.04	0.03				
CaO	0.11	0.08	0.09	0.16	0.11	0.14	0.11	0.09	0.07	0.13	0.12	0.15	0.1	0.12	0.19	0.14	0.14				
MgO	0.06	0.07	0.06	0.62	0.09	0.25	0.11	0.07	0.09	0.18	0.09	0.08	0.07	0.26	0.53	0.41	1.37				
K <sub>2</sub> O	0.06	0.07	0.08	0.03	0.06	0.1	0.06	0.04	0.04	0.07	0.04	0.06	0.1	0.01	0.08	0.11	0.07				
Na <sub>2</sub> O	0.002	0.002	0.002	0.002	0.002	0.002	0.002	0.002	0.002	0.002	0.002	0.01	0.01	0.01	0.013	0.02	0.002				
MnO	0.03	0.07	0.09	0.17	0.11	0.16	0.04	0.17	0.09	0.05	0.17	0.06	0.06	0.23	0.21	0.04	0.45				
TiO <sub>2</sub>	0.02	0.01	0.02	0.02	0.01	0.03	0.01	0.01	0.02	0.02	0.01	0.02	0.01	0.02	0.02	0.03	0.03				
P <sub>2</sub> O <sub>5</sub>	0.51	0.3	0.61	0.91	0.5	2.05	1.0	0.47	0.69	1.16	0.88	0.21	0.75	1.05	1.54	1.05	0.75				
LOI	99.85	99.73	99.98	99.77	100.01	99.83	99.79	100.03	99.64	99.65	99.96	99.94	99.66	100.25	99.62	99.93	100.07				
Total	84	82	88	79	80	91	91	89	88	90	93	76	89	88	86	84	66				
CIA																					

Lithology	Lower conglomerate															Basal arenite						Schist		
	115.8	127.8	136.8	150.2	156.7	157.5	162.35	168	168.35	171.45	177.1	181.4	185	187	188.65	200.65	222.45							
Depth (m)	90.05	85.64	90.45	90.38	90.55	86.69	79.79	90.66	90.54	89.41	53.51	79.72	89.26	92.53	44.16	48.42	63.94							
SiO <sub>2</sub>	4.41	6.82	5.04	4.94	4.51	6.76	7.08	4.61	4.7	5.51	22.2	8.99	3.88	2.61	15.63	20.63	14.26							
Al <sub>2</sub> O <sub>3</sub>	1.69	1.78	0.62	0.95	0.83	1.35	5.48	0.33	0.72	0.6	6.42	4.05	3.4	1.91	18.57	12.48	8.33							
Fe <sub>2</sub> O <sub>3</sub>	0.02	0.03	0.03	0.02	0.02	0.03	0.03	0.01	0.02	0.02	0.09	0.04	0.03	0.01	1.68	1.82	1.24							
CaO	0.14	0.2	0.13	0.13	0.18	0.24	0.27	0.16	0.23	0.24	0.86	0.77	0.68	0.22	4.85	4.73	3.86							
MgO	2.4	4.25	2.89	2.19	2.67	3.78	3.3	3.25	2.86	3.07	9.37	2.97	1.27	1.36	0.71	3.44	1.96							
K <sub>2</sub> O	0.07	0.13	0.12	0.08	0.16	0.12	0.07	0.14	0.07	0.15	0.08	0.12	0.13	0.1	3.24	3.02	2.68							
Na <sub>2</sub> O	0.002	0.002	0.002	0.002	0.002	0.002	0.002	0.002	0.002	0.002	0.01	0.03	0.04	0.002	0.26	0.19	0.1							
MnO	0.23	0.12	0.02	0.04	0.09	0.06	0.15	0.1	0.09	0.07	0.6	0.37	0.05	0.09	3.96	0.94	0.69							
TiO <sub>2</sub>	0.02	0.02	0.02	0.01	0.02	0.02	0.02	0.02	0.01	0.02	0.02	0.03	0.02	0.01	1.13	0.17	0.13							
P <sub>2</sub> O <sub>5</sub>	1.08	0.86	0.65	1.21	0.98	0.84	3.66	0.65	0.79	1.04	6.29	2.85	1.35	1.2	5.05	4.1	2.66							
LOI	100.11	99.85	99.97	99.95	100.03	99.89	99.85	99.93	100.03	100.13	99.45	99.94	100.11	100.04	99.24	99.94	99.85							
Total	62	58	60	66	59	61	65	55	59	60	68	72	70	61	63	63	62							
CIA																								

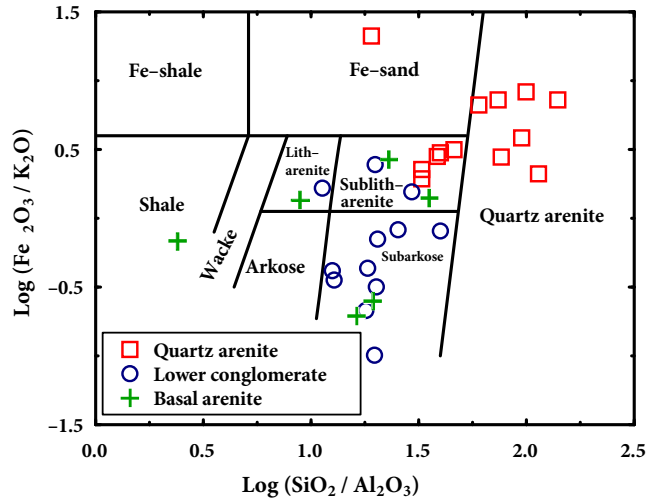


**Figure 4.** Geochemical classification of the clastic rocks of the Kerur Formation using  $\text{log}(\text{SiO}_2/\text{Al}_2\text{O}_3) - \text{log}(\text{Fe}_2\text{O}_3/\text{K}_2\text{O})$  diagram (after Herron, 1988).

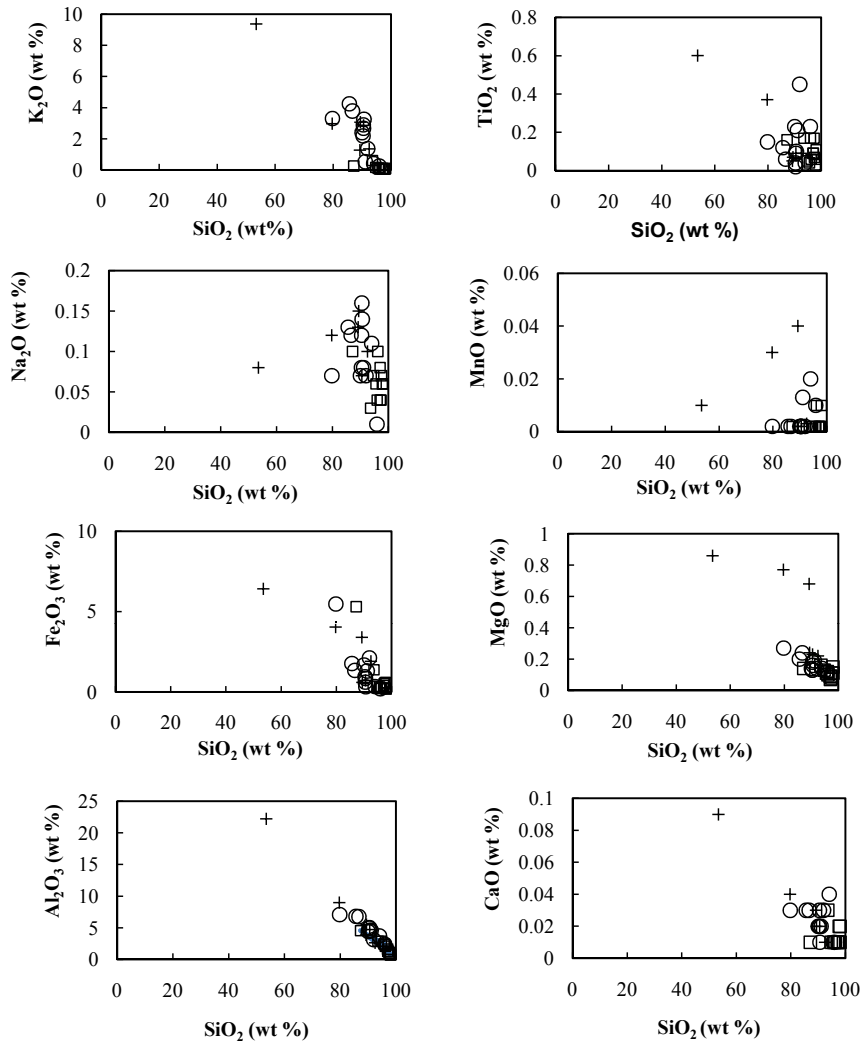


**Figure 5.** Variations of  $\text{SiO}_2$  versus  $\text{Al}_2\text{O}_3$ ,  $\text{Fe}_2\text{O}_3$ ,  $\text{Na}_2\text{O}$ ,  $\text{K}_2\text{O}$ ,  $\text{CaO}$ ,  $\text{MgO}$ ,  $\text{MnO}$ , and  $\text{TiO}_2$  (wt %) for clastic rocks of the Kerur Formation.

**Table 3.** Trace element concentrations (ppm) in the clastic rocks of the Kerur Formation.

Lithology	Quartz arenites									Lower conglomerate			
	2.0	8.4	13.8	35	52.8	58.8	64.8	70.55	73.1	77.5	87.75	97.8	115.8
Sc	1.4	1.4	1.5	1.5	1.7	1.6	1.5	1.4	1.5	1.4	1.7	1.4	1.4
V	5.67	7.42	8.54	4.07	59.21	6.56	4.52	8.94	4.87	7.62	21.05	7.91	13.91
Cr	9.5	9.7	10.2	9.8	92.39	15.95	10.3	9.4	9.8	13.92	42.89	15.77	19.92
Co	0.32	0.39	0.62	0.34	4.31	0.5	0.4	0.4	0.72	0.37	1.04	2.07	2.82
Ni	1.9	1.9	2.42	1.9	11.38	2.09	2.0	1.9	1.9	1.8	4.86	4.10	4.77
Cu	1.98	2.16	4.41	2.0	116	2.64	2.56	2.76	1.18	5.33	8.83	42.1	6.28
Zn	0.58	1.16	2.36	2.37	32.11	2.81	0.79	1.66	1.71	2.33	5.51	4.86	5.66
Rb	1.77	1.94	1.91	3.14	8.37	3.8	3.17	3.31	2.31	11.05	24.57	17.31	80.23
Sr	5.31	4.13	3.2	2.99	5.96	2.35	2.8	3.07	4.15	3.52	9.63	10.45	32.81
Y	4.76	4.09	7.99	4.45	8.15	8.1	3.15	3.4	3.48	4.52	11.35	8.78	11.64
Zr	84	70	140	105	180	249	69	57	34	90	246	179	181
Nb	0.76	0.85	1.11	1.14	2.36	2.02	0.79	0.81	1.0	1.08	4.37	4.71	6.35
Cs	0.06	0.06	0.06	0.10	0.36	0.12	0.1	0.15	0.09	0.26	0.98	0.88	3.54
Ba	18	20	15	15	54	16	17	18	20	19	68	89	279
Hf	2.12	1.85	3.5	2.69	4.48	6.11	1.78	1.59	0.88	2.26	6.26	5.15	4.66
Ta	0.06	0.08	0.11	0.05	0.27	0.2	0.08	0.09	0.1	0.17	0.58	0.7	1.03
Pb	5.08	4.65	1.07	1.78	19.89	5.40	3.7	5.93	2.71	2.25	6.87	6.45	10.66
Th	0.89	0.75	1.36	1.12	3.71	4.24	1.61	2.7	0.55	4.18	12.22	19.11	29.92
U	0.46	0.55	0.93	0.7	5.72	4.57	1.35	1.18	0.39	3.36	4.18	3.14	4.04

**Table 3.** Continued.

Lithology	Lower conglomerate					Basal arenite				Schist		
	127.8	150.2	157.5	162.35	168	171.45	177.1	181.4	185	188.65	200.65	222.45
Sc	1.5	1.3	1.5	1.46	1.5	1.4	9.81	5.96	1.4	17.44	19.22	8.88
V	15.49	10.32	14.65	25.02	11.22	18.79	131.84	49.78	17.88	146.27	168.04	81.21
Cr	12.37	9.0	13.05	57.23	42.23	30.82	78.78	59.82	9.3	9.9	162.44	80.77
Co	1.58	0.7	1.5	3.44	11.93	6.7	20.73	29.64	23.54	63.68	39.52	12.93
Ni	6.18	3.29	6.56	9.44	12.66	11.16	29.36	49.55	23.34	33.45	101.44	46.77
Cu	0.67	0.6	0.71	0.66	8.67	1.63	12.12	74.33	2.43	15.97	19.92	8.92
Zn	3.98	2.39	4.42	7.78	2.92	13.88	26.91	46.44	43.92	209.87	113.66	49.01
Rb	115.97	62.95	122.66	123.51	98.4	92.73	292.55	123.07	37.76	26.65	108.32	40.46
Sr	63.41	28.78	49.48	33.14	50.93	40.12	66.62	36	14.01	143.34	179.49	91.46
Y	6.64	4.32	4.21	6.68	7.39	4.81	18.42	16.54	3.44	60.58	27.15	14.89
Zr	115	47	68	97	149	76	303	260	39	552	275	139
Nb	2.84	0.91	1.6	2.64	2.22	1.28	8.94	4.28	0.71	39.45	11.4	5.78
Cs	1.74	1.34	2.3	5.95	1.77	2.43	15.91	6.24	0.86	1.68	6.79	1.84
Ba	661	237	449	290	469	384	787	368	153	192	722	249
Hf	3.17	1.33	1.81	2.6	3.69	2.05	7.57	6.26	1.04	12.32	6.74	3.36
Ta	0.43	0.19	0.2	0.29	0.60	0.15	1.06	0.44	0.06	3.0	1.2	0.57
Pb	14.36	8.67	10.96	8.45	13.19	8.95	21.52	7.43	3.66	5.15	48.97	7.17
Th	10.37	3.66	5.06	5.91	7.92	4.06	16.15	8.34	1.02	4.42	16.15	7.37
U	1.75	1.21	0.91	6.97	1.99	1.22	5.19	1.89	0.34	1.3	5.03	1.86

largely fixed in the k-feldspar and clay minerals. However, the correlation of  $Al_2O_3$  and  $K_2O$  versus Rb, Ba, and Sr is poor or negative for quartz arenites ( $Al_2O_3$ :  $r = 0.25$ ,  $r = 0.09$ ,  $r = -0.13$ , respectively;  $K_2O$ :  $r = 0.17$ ,  $r = -0.04$ ,  $r = -0.28$ , respectively). This suggests that the distributions of these elements are not controlled by k-feldspar and clays in the quartz arenites.

The results of REE analysis are given in Table 4, and chondrite-normalized patterns are shown in Figure 7.  $\Sigma$ REE concentrations vary widely, which is characteristic of individual rock types, e.g., basal arenite (~7.84–74.98 ppm;  $n = 4$ ), lower conglomerate (~18.84–158.66 ppm;  $n = 9$ ), and quartz arenite (~12.96–43.06 ppm;  $n = 9$ ). All analyzed samples have  $\Sigma$ REE abundances less than



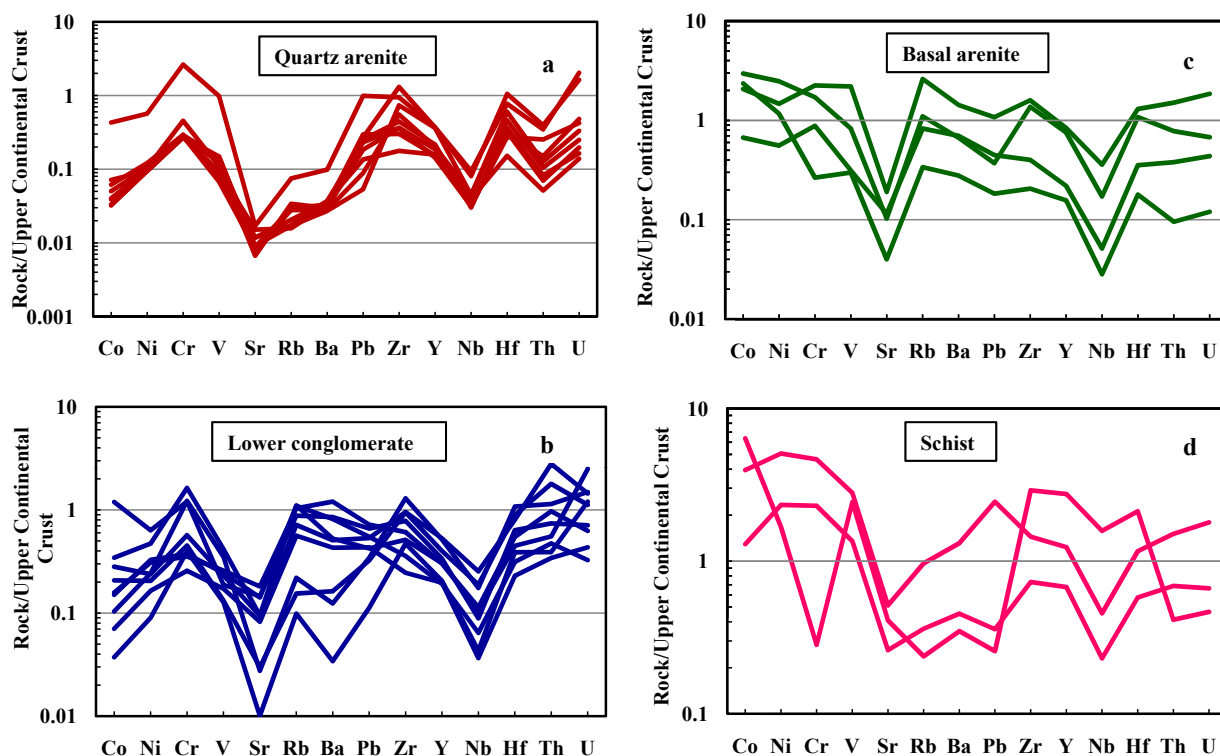


**Figure 6.** a) UCC-normalized trace elements diagram for quartz arenite of the Kerur Formation, b) UCC-normalized trace elements spider diagram for lower conglomerate samples of the Kerur Formation, c) UCC-normalized trace elements diagram for basal arenite samples, d) UCC-normalized spider diagram for basement schist rocks collected from the DNR-58 core.

the average UCC (~143; Taylor and McLennan, 1985). The REE patterns of the samples studied are light REE (LREE)-enriched ( $La_{CN}/Sm_{CN} = 7.73 \pm 2.38$ ,  $n = 25$ ), with relatively flat heavy REE (HREE) ( $Gd_{CN}/Yb_{CN} = 2.61 \pm 0.67$ ,  $n = 25$ ) and a negative Eu anomaly ( $Eu/Eu^* = 0.77 \pm 0.38$ ). The samples from lower conglomerate and basal arenite show negative or mildly positive Eu anomalies ( $Eu/Eu^* = 0.38$ – $1.10$ ,  $0.75$ – $1.13$ , respectively), whereas quartz arenites display significant negative Eu anomalies ( $Eu/Eu^* = 0.57$ – $0.77$ ). A small enrichment of HREEs in some samples of the Kerur Formation can be due to the inclusion of phases that retain HREEs (e.g., zircon). The correlation between  $\Sigma REE$  and  $Al_2O_3$  for quartz arenite and lower conglomerate is not statistically significant ( $r = -0.21$ ,  $r = -0.27$ , respectively), indicating that REEs are mainly concentrated in the accessory minerals rather than in clay minerals. On the other hand, basal arenites have significant correlation between  $\Sigma REE$  and  $Al_2O_3$  contents ( $r = 0.72$ ), suggesting that REEs are probably hosted by clay minerals.

## 5. Discussion

### 5.1. Paleoweathering

Chemical weathering strongly affects the major-element geochemistry and mineralogy of siliclastic sediments

(Nesbitt and Young, 1982, 1984; Johnsson et al., 1988; McLennan et al., 1993, 2004; Fedo et al., 1995), where larger cations ( $Al_2O_3$ , Ba, Rb) remain fixed in the weathering profile preferentially over smaller cations (Ca, Na, Sr), which are selectively leached (Nesbitt et al., 1980). These chemical signatures are ultimately transferred to the sedimentary record (e.g., Nesbitt and Young, 1982; Wronkiewicz and Condie, 1987), thus providing a useful tool for monitoring source-area weathering conditions. Quantitative measures, such as the CIA (Nesbitt and Young, 1982), the plagioclase index of alteration (PIA) (Fedo et al., 1996), the chemical index of weathering (CIW) (Harnois, 1988), and the index of compositional variability (ICV) (Cox et al., 1995), are used to interpret the degree of chemical weathering and to trace the source rocks and provenance of sediments (Fedo et al., 1995; Cullers and Podkovyrov, 2000; Lamaskin et al., 2008; Dostal and Keppie, 2009). Among them, the CIA (Nesbitt and Young, 1982) is widely used to determine the degree of source-area weathering. The CIA values are determined using molecular proportion from the formula  $CIA = [Al_2O_3 / (Al_2O_3 + CaO^* + Na_2O + K_2O)] \times 100$ , where  $CaO^*$  represents CaO associated with silicate phases. The CaO content in most of the samples studied is very low and therefore the total CaO content is used as  $CaO^*$  in the calculation of the CIA value. Higher CIA values indicate

intense chemical weathering (Nesbitt and Young, 1982; Fedo et al., 1995), whereas low CIA values suggest the near absence of chemical alteration and therefore might reflect cool and/or arid conditions (Fedo et al., 1995).

The CIA values vary from 58 to 95. For each lithology the CIA values vary as follows: basal arenite (61–74), lower conglomerate (58–90), and quartz arenite (81–95). During the initial stage of weathering, the sediments derived from the various igneous rocks (trend lines 1–5; Figure 8) mainly plot parallel to the A-CN line because Na<sub>2</sub>O and CaO are leached out from the earlier dissolved plagioclase. Increasing weathering intensity of the source rocks leads to the destruction of plagioclase. This resulted in the loss of Ca and Na from plagioclase feldspar and the resulted sediments plot closer to the A-K axis (e.g., Descourvieres et al., 2011; Misra and Sen, 2012; Raza et al., 2012). Likewise, the intensely weathered samples plot nearer to apex A, suggesting the abundance of kaolinite and gibbsite over primary minerals such as feldspar. Interestingly, samples of basal arenite, lower conglomerate, and quartz arenite are clustered at two points. In the A-CN-K diagram, quartz arenites and few lower conglomerate

samples plot closer to apex A, indicating that these sediments underwent intense chemical weathering in the source region. However, most of the lower conglomerate and basal arenite samples follow the A-K trend line and plot between k-feldspar and muscovite fields, implying that their source area experienced moderate intensity of chemical weathering. This is also supported by PIA values (Fedo et al., 1995), which are obtained using the following equation (molecular proportion):  $PIA = [Al_2O_3 - K_2O] / (Al_2O_3 + CaO^* + Na_2O - K_2O) \times 100$ . The PIA values are more or less similar to CIA values.

In the A-CN-K compositional space, each lithology exhibits a wide range of CIA values, and the observed compositional diversity is interpreted to reflect temporal variations in the balance between erosion and chemical weathering. Because the degree of weathering is chiefly a function of climate and tectonic-uplift rates (Wronkiewicz and Condie, 1987), increased chemical weathering intensity might reflect a decrease in tectonic activity and/or a change in climate toward warm and humid conditions (Jacobson et al., 2003). Therefore, weathering indices of sedimentary rocks can provide useful information about

**Table 4.** Rare earth element concentrations (ppm) and their ratios in the clastic rocks of the Kerur Formation.

Lithology	Quartz arenites									Lower conglomerate			
	2.0	8.4	13.8	35	52.8	58.8	64.8	70.55	73.1	77.5	87.75	97.8	115.8
La	8.62	3.41	5.37	2.63	9.44	4.15	2.86	4.12	4.07	3.99	25.35	25.50	35.93
Ce	13.68	6.89	9.58	5.55	18.53	8.85	5.34	6.42	6.46	7.68	42.65	39.73	72.18
Pr	1.72	0.73	0.90	0.55	1.73	0.92	0.51	0.60	0.71	0.78	4.18	3.66	7.48
Nd	7.22	2.84	3.22	2.19	6.62	3.54	1.85	2.20	2.65	2.92	15.86	13.24	28.22
Sm	1.21	0.60	0.69	0.50	1.40	0.91	0.43	0.53	0.55	0.65	2.93	2.42	4.99
Eu	0.25	0.15	0.20	0.13	0.31	0.23	0.09	0.10	0.13	0.11	0.43	0.28	0.61
Gd	1.07	0.69	0.97	0.57	1.36	1.14	0.47	0.54	0.60	0.70	2.53	2.13	3.86
Tb	0.16	0.12	0.20	0.11	0.23	0.20	0.08	0.09	0.10	0.13	0.40	0.31	0.47
Dy	0.80	0.68	1.26	0.64	1.25	1.13	0.47	0.51	0.58	0.71	1.85	1.45	1.90
Ho	0.16	0.14	0.29	0.13	0.26	0.24	0.10	0.10	0.12	0.14	0.37	0.28	0.36
Er	0.54	0.44	1.03	0.44	0.81	0.79	0.31	0.33	0.40	0.45	1.13	0.87	1.12
Tm	0.08	0.07	0.16	0.06	0.12	0.12	0.05	0.05	0.06	0.06	0.17	0.14	0.17
Yb	0.62	0.49	1.18	0.46	0.86	0.87	0.33	0.35	0.43	0.45	1.24	0.94	1.20
Lu	0.10	0.08	0.19	0.07	0.13	0.15	0.05	0.06	0.07	0.07	0.20	0.15	0.19
Th/U	1.94	1.35	1.46	1.60	0.65	0.93	1.19	2.28	1.42	1.24	2.92	6.09	7.40
La/Th	9.70	4.56	3.96	2.34	2.54	0.98	1.78	1.52	7.37	0.95	2.07	1.32	1.20
La/Co	26.66	8.72	8.70	7.84	2.19	8.24	7.17	10.24	5.68	10.70	24.43	12.16	12.76
Th/Co	2.75	1.91	2.20	3.35	0.86	8.43	4.02	6.72	0.77	11.21	11.78	9.22	10.63
La/Sc	6.16	2.44	3.58	1.75	5.56	2.59	1.91	2.94	2.71	2.85	14.92	18.00	25.66
Th/Sc	0.64	0.54	0.90	0.75	2.19	2.65	1.07	1.93	0.37	2.98	7.19	13.65	21.37
Th/Cr	0.09	0.08	0.13	0.11	0.04	0.27	0.16	0.29	0.06	0.30	0.29	1.21	1.50
Rb/Sr	0.33	0.47	0.60	1.05	1.40	1.62	1.13	1.08	0.56	3.14	2.55	1.66	2.45
Cr/Th	10.68	12.94	7.52	8.73	24.88	3.76	6.41	3.48	17.76	3.33	3.51	0.83	0.67
SLREE/SHREE	9.18	5.35	3.74	4.60	7.50	3.96	5.89	6.83	6.10	5.90	11.56	13.45	16.08
SREE	36.23	17.34	25.25	14.01	43.06	23.24	12.96	16.01	16.94	18.84	99.28	90.80	158.66
(La/Yb) <sub>cn</sub>	9.35	4.68	3.09	3.88	7.44	3.23	5.81	7.98	6.39	6.02	13.86	18.16	20.31
(La/Sm) <sub>cn</sub>	4.50	3.56	4.87	3.33	4.26	2.87	4.23	4.90	4.63	3.88	5.44	6.56	4.53
(Gd/Yb) <sub>cn</sub>	1.39	1.14	0.67	1.01	1.29	1.07	1.14	1.25	1.12	1.26	1.66	1.84	2.61
Eu/Eu*	0.68	0.72	0.75	0.77	0.69	0.68	0.64	0.57	0.71	0.49	0.49	0.38	0.42

Table 4. (Continued).

Lithology	Lower conglomerate					Basal arenite				Schist		
	127.8	150.2	157.5	162.35	168	171.45	177.1	181.4	185	188.65	200.65	222.45
La	11.47	2.40	7.63	6.92	9.35	6.68	15.11	16.20	1.43	74.88	37.44	16.45
Ce	16.86	5.40	12.00	8.17	20.77	12.13	27.95	31.13	2.90	155.23	71.03	31.77
Pr	1.72	0.62	1.23	0.69	2.16	1.18	2.97	3.04	0.33	19.42	7.27	3.31
Nd	6.32	2.48	4.53	2.25	8.01	4.22	11.40	11.67	1.12	87.08	27.85	13.32
Sm	1.22	0.63	0.84	0.56	1.44	0.79	2.36	2.25	0.28	16.53	5.08	2.65
Eu	0.34	0.21	0.26	0.23	0.41	0.26	0.68	0.54	0.11	4.67	1.23	0.76
Gd	1.18	0.65	0.77	0.75	1.28	0.79	2.61	2.16	0.30	14.79	4.67	2.72
Tb	0.19	0.12	0.12	0.15	0.21	0.13	0.50	0.42	0.06	2.31	0.81	0.46
Dy	1.03	0.67	0.65	0.96	1.10	0.71	2.86	2.48	0.43	10.60	4.39	2.45
Ho	0.20	0.13	0.13	0.21	0.23	0.15	0.59	0.55	0.10	2.01	0.94	0.50
Er	0.65	0.42	0.41	0.66	0.74	0.51	1.93	1.88	0.34	5.76	3.00	1.54
Tm	0.10	0.06	0.07	0.10	0.11	0.08	0.29	0.29	0.05	0.77	0.46	0.22
Yb	0.72	0.42	0.45	0.67	0.79	0.56	2.04	2.06	0.34	5.20	3.27	1.58
Lu	0.12	0.07	0.08	0.11	0.12	0.09	0.32	0.32	0.06	0.77	0.50	0.23
Th/U	5.91	3.02	5.55	0.85	3.99	3.32	3.11	4.40	3.03	3.40	3.21	3.97
La/Th	1.11	0.66	1.51	1.17	1.18	1.65	0.94	1.94	1.40	16.92	2.32	2.23
La/Co	7.25	3.40	5.09	2.01	0.78	1.00	0.73	0.55	0.06	1.18	0.95	1.27
Th/Co	6.55	5.20	3.37	1.72	0.66	0.61	0.78	0.28	0.04	0.07	0.41	0.57
La/Sc	7.65	1.84	5.09	4.73	6.24	4.77	1.54	2.72	1.02	4.29	1.95	1.85
Th/Sc	6.91	2.81	3.37	4.04	5.28	2.90	1.65	1.40	0.73	0.25	0.84	0.83
Th/Cr	0.84	0.41	0.39	0.10	0.19	0.13	0.21	0.14	0.11	0.45	0.10	0.09
Rb/Sr	1.83	2.19	2.48	3.73	1.93	2.31	4.39	3.42	2.69	0.19	0.60	0.44
Cr/Th	1.19	2.46	2.58	9.69	5.33	7.60	4.88	7.17	9.12	2.24	10.06	10.96
ΣREE/SHREE	8.96	4.56	9.81	5.14	9.13	8.29	5.37	6.33	3.61	8.37	8.24	6.95
SREE	42.14	14.27	29.16	22.46	46.71	28.28	71.60	74.98	7.84	400.02	167.94	77.98
(La/Yb) <sub>cn</sub>	10.73	3.84	11.42	6.94	8.04	8.04	5.01	5.31	2.84	9.74	7.73	7.03
(La/Sm) <sub>cn</sub>	5.94	2.38	5.72	7.73	4.10	5.29	4.03	4.53	3.26	2.85	4.64	3.90
(Gd/Yb) <sub>cn</sub>	1.32	1.24	1.37	0.90	1.31	1.14	1.04	0.85	0.72	2.31	1.16	1.39
Eu/Eu*	0.88	0.99	0.99	1.10	0.92	1.02	0.83	0.75	1.13	0.91	0.77	0.86

tectonic activity and climatic conditions in the source area. In this study, most of the samples show moderate to high CIA values, which are interpreted to reflect a steady state of weathering, probably under tropical to subtropical conditions (Nesbitt et al., 1997).

Sedimentary recycling can be identified using Rb/Sr ratios, where Sr easily leaches compared to Rb and this leads to a significant increase in the Rb/Sr ratio, and high ratios have been interpreted to be indicators of strong weathering and sediment recycling (McLennan et al., 1993). The Rb/Sr ratios of the basal arenite, lower conglomerate, and quartz arenites (0.33 to 1.62, 1.66 to 3.73, and 2.31 to 4.39, respectively) are higher than the average PAAS value (0.80; Taylor and McLennan, 1985). The high CIA values and Rb/Sr ratios suggest moderate to intense weathering in the source region.

## 5.2. Hydraulic sorting

Hydraulic sorting might lead to a significant difference in REE concentrations in sediments and sedimentary rocks with different mineral contents and grain-sized variations (e.g., Cullers et al., 1975, 1979; Gromet et al., 1984; McLennan, 1989; Singh, 2009; Wu et al., 2013).

The ΣREE content in the clastic rocks is affected by size sorting, and the ΣREE content decreases steadily with an increase in grain size (Cullers and Stone, 1991). Three major factors associated with sedimentary sorting that affect REE patterns in clastic rocks are grain size contrast, general mineralogy, and heavy mineral fractionation. A strong assumption about the sorting processes during sedimentation is that fine-grained sediments tend to have a relative abundance of REE, as found in their source region (Haskin et al., 1966; McCulloch and Wasserburg, 1978; McLennan and Taylor, 1982; McLennan et al., 1990; Cullers, 1995).

In the present study, different lithologies show large variations in ΣREE content that might be due to either grain size variations or the inclusion of heavy mineral fractions. The sedimentary rocks studied show large variations in grain size; for example, conglomerate samples show coarse-grained sediments, whereas arenites show fine- to medium-grained fractions. If the observed variations in ΣREE contents in these sedimentary rocks are largely due to grain-size variations, then the conglomerate

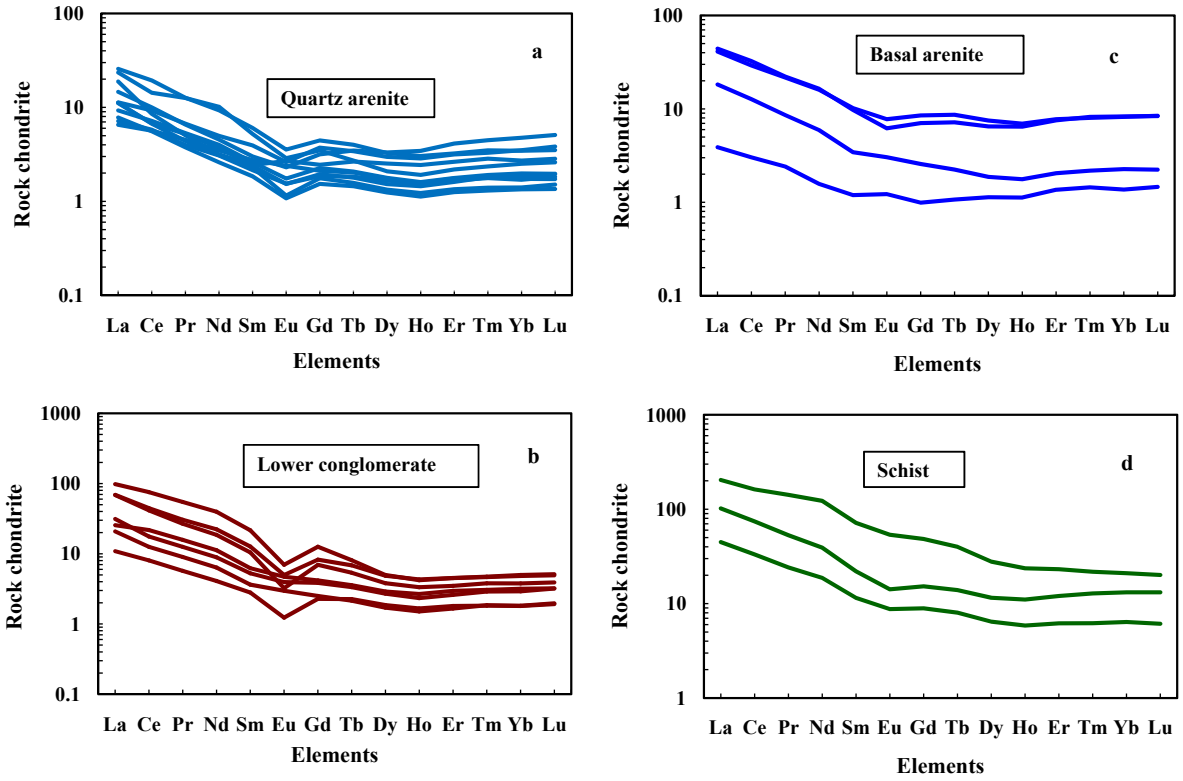


**Figure 7.** a) Chondrite-normalized REE patterns for quartz arenite samples, b) chondrite-normalized REE patterns for lower conglomerate of the Kerur Formation, c) chondrite-normalized REE patterns for basal arenite, d) chondrite-normalized REE patterns for basement schist rock.

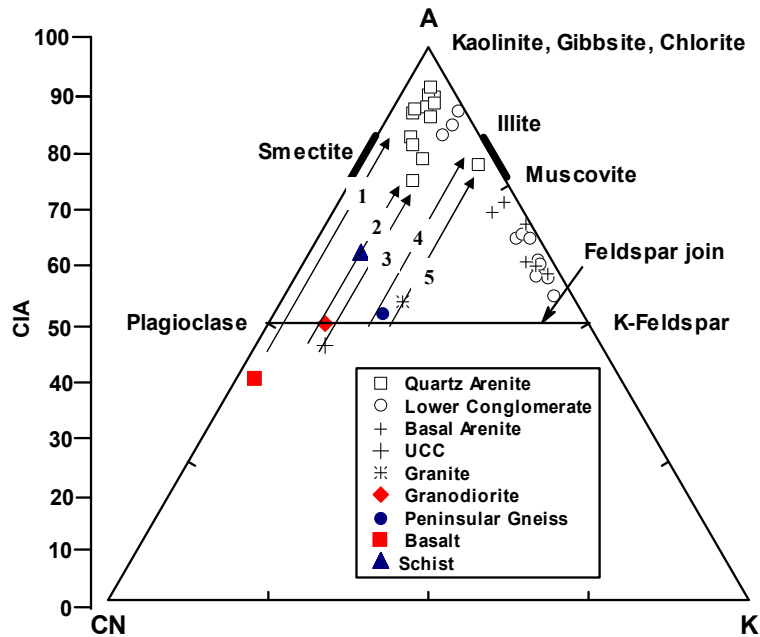


**Figure 8.** A-CN-K diagram showing the weathering trend of the Kerur Formation (after Nesbitt and Young, 1982). A:  $Al_2O_3$ ; CN:  $CaO + Na_2O$ ; K:  $K_2O$  (molecular proportions). Trend lines 1-5: weathering trends; UCC and basalt data from Condie (1993); peninsular gneiss: Allen (1985); granite and granodiorite: Jayananda (2000); schist: present study.

units should show lower  $\Sigma$ REE content than the arenites, but many conglomerate samples show elevated  $\Sigma$ REE content compared to the fine-grained lithologies. As such, the variations in  $\Sigma$ REE content in these litho-units might not be due to grain-size variations. The inclusions of small portions of heavy minerals can drastically change the  $\Sigma$ REE contents in the sedimentary rocks. Thus, the sedimentary rocks studied indicate the presence of various proportions of heavy minerals (zircon, tourmaline, rutile, garnet, magnetite, and ilmenite). The petrographic study of conglomerate and quartz arenite samples reveals the presence of heavy minerals in them.

Cox et al. (1995) proposed a new formula, the ICV, to understand the geochemical variability due to hydraulic sorting. Rock-forming minerals such as k-feldspars, plagioclase, amphiboles, and pyroxenes display higher ICV values ( $>0.84$ ), whereas alteration products such as kaolinite, illite, and muscovite show lower values ( $<0.84$ ; Cox et al., 1995; Cullers, 2000). For the Kerur Formation, the ICV values vary between 0.26 and 1.44. For each lithology the ICV values vary as follows: basal arenite (0.75–1.44), lower conglomerate (0.30–1.34), and quartz arenite (0.26–1.37), indicating that these rocks contain unequal proportions of both clay minerals and nonclay silicate minerals.

A statistically significant positive correlation of Zr with Yb ( $r = 0.72$ ,  $r = 0.95$ ,  $r = 0.99$ , respectively) and HREEs ( $r = 0.80$ ,  $r = 0.89$ ,  $r = 0.99$ , respectively) for the basal arenite, lower conglomerate, and quartz arenite suggests that the HREE fractionation is controlled mainly by the concentration of zircon mineral. The basal arenite, lower conglomerate, and quartz arenite show wide variations in Zr and Hf contents. McLennan et al. (1993) observed that the Th/Sc ratio is a sensitive index of the bulk composition of the provenance, and the Zr/Sc ratio is a useful index of zircon enrichment. In the Zr/Sc versus Th/Sc diagram (Figure 9), the samples are plotted to identify the role of heavy mineral concentrations during sediment sorting. In this diagram (Figure 9), the studied samples display two compositional trends with some samples plotting along Trend 1, which is indicative of a minimal influence of mineral sorting. Samples plotting along Trend 2 are indicative of zircon enrichment by sediment recycling and sorting. This suggests that the geochemical compositions of lower conglomerate and quartz arenite are exaggerated by sorting effects.

### 5.3. Provenance

The geochemical signatures of clastic sediments have been used to determine provenance (Taylor and McLennan, 1985; Cullers, 1995; Madhavaraju and Ramasamy, 2002; Armstrong-Altrin et al., 2004, 2013; Al-Juboury and Al-Hadidy, 2009; Perri et al., 2011; Shadan and Hosseini-Barzi, 2013; Madhavaraju, 2015). Elements concentrated

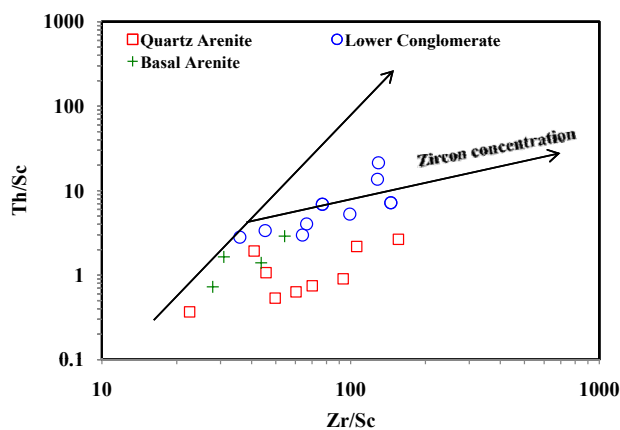


**Figure 9.** Zr/Sc vs. Th/Sc bivariate diagram (McLennan et al., 1993).

in mafic (Sc, Cr, and Co) and in silicic (La, Th, and REE) sediments, REE patterns, and the size of the Eu anomaly have been used widely to understand the provenance signatures' interpretation (e.g., Shynu et al., 2011). REEs and certain trace elements (Th, Sc, and Cr) can provide an insight into the provenance and are thus useful to constrain the average source-area composition (e.g., Taylor and McLennan, 1985; Floyd et al., 1989; McLennan et al., 1993; Fedo et al., 1996; Cullers and Berendsen, 1998).

$Al_2O_3/TiO_2$  ratios in clastic sediments can be used to identify the source rock composition (Garcia et al., 1994; Andersson et al., 2004). The Al in igneous rocks resides mostly in feldspars and Ti in mafic minerals (e.g., olivine, pyroxene, hornblende, biotite, and ilmenite) and the  $Al_2O_3/TiO_2$  ratios increase from 3 to 8 in mafic igneous rocks, from 8 to 21 in intermediate igneous rocks, and from 21 to 70 in felsic igneous rocks (Hayashi et al., 1997). In general, the variation in the  $Al_2O_3/TiO_2$  ratio (12 to 252) suggests that the samples were derived from intermediate to felsic source rocks. However, two samples from lower conglomerate and two samples from quartz arenite show a low  $Al_2O_3/TiO_2$  ratio (Table 2), which may be due to increasing sediment maturity and/or the presence of a significant amount of  $TiO_2$ -rich minerals (ilmenite, anatase, brookite, and rutile).

The abundance of Cr and Ni in siliciclastic sediments is considered as a useful indicator in provenance studies. The higher concentration of Cr and Ni (Cr:  $>150$  ppm, Ni:  $>100$  ppm) and low ratios of Cr/Ni (1.3–1.5) suggest the ultramafic signatures of the source rocks (Garver et al., 1996). In the present study, the samples studied show low Cr and Ni content (Cr: 9.00–92.39 ppm, Ni: 1.8–49.55 ppm) when compared with ultramafic source rocks. In addition, they also show wide variations in the Cr/Th ratio, which ranges from 0.67 to 24.88, with an average of 7.11. The Cr and Ni contents and Cr/Th ratio observed in the sedimentary rocks strongly support the felsic nature of

the source rocks. In addition, the Cr/V ratio is an index of the enrichment of Cr over the other ferromagnesian trace elements, whereas Y/Ni monitors the general level of ferromagnesian trace elements (Ni) compared to a proxy for HREEs (Y). Mafic sources have high ferromagnesian abundances; such a provenance would result in a decrease in Y/Ni (e.g., Hiscott, 1984; McLennan et al., 1993). The Cr/V vs. Y/Ni diagram (Hiscott, 1984) indicates the lack of mafic detritus input for the studied samples (Figure 10).

The La/Sc versus Th/Co bivariate plot is more useful to understand the source rock information of the clastic rocks (Cullers, 2002). In the present study, most of the samples fall in the felsic field rather than the mafic field, which strongly supports the felsic nature of the source rocks (Figure 11). In addition, La-Th-Sc triangular diagrams can provide information regarding the source rock characteristics (McLennan and Taylor, 1991; Cullers, 2002). In this diagram, most of the samples plot near the granite and granodiorite fields (Figure 12), suggesting that the sedimentary rocks were mainly derived from the granite and granodioritic rocks of the source region.

The REE patterns and the size of the Eu anomalies in the sediments provide useful information regarding source rock characteristics (Taylor and McLennan, 1985), since mafic igneous rocks have low LREE/HREE ratios and little or no negative Eu anomalies, whereas felsic igneous rocks have higher LREE/HREE ratios and negative Eu anomalies (Cullers, 1994a, 1994b). In the present study, most of the sedimentary rocks show higher LREE/HREE ratios and negative Eu anomalies, whereas few samples show a positive Eu anomaly, which suggests the felsic nature of the source rocks. The low positive Eu anomaly in few samples is likely due to inclusion of more feldspar in these samples.

Elemental ratios such as La/Sc, Th/Sc, La/Co, Th/Co, Th/Cr, Cr/Th, and Eu/Eu\* show remarkable variations in felsic and mafic rocks, which are highly useful in unravelling the provenance signatures of the sedimentary

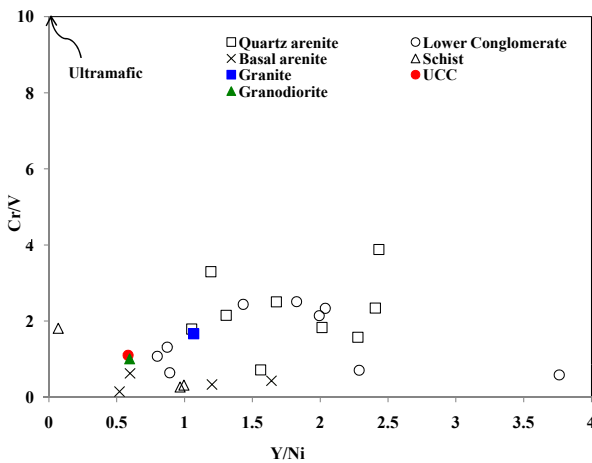


Figure 10. Y/Ni vs. Cr/V bivariate plot.

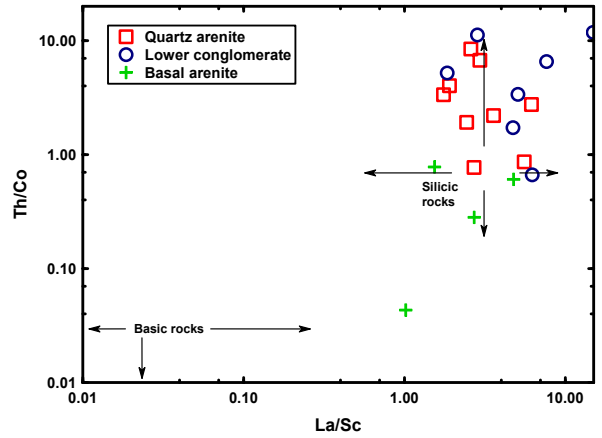


Figure 11. La/Sc vs. Th/Co bivariate plot (after Cullers, 2002).

rocks (Wronkiewicz and Condie, 1987, 1989, 1990; Cullers et al., 1988; Cullers, 1994b, 1995; Cox et al., 1995; Armstrong-Altrin et al., 2004; Nagarajan et al., 2007a, 2007b, 2011; Madhavaraju and Lee, 2009, 2010; Madhavaraju et al., 2010, 2015). The La/Sc, La/Co, Th/Co, Th/Cr, Cr/Th, and Th/Sc ratios of the sedimentary rocks in this study have been compared with felsic and mafic rocks (fine fraction) and UCC values (Table 5) to discover the source rock characteristics. It suggests that these rocks were derived from felsic source rocks.

The intracratonic Kaladgi basin had considerable asymmetry between the northern and southern margins in terms of source composition and tectonics (Dey et al., 2009). During the initial stage, the northern part of the basin received more arkosic sediments from K-rich granitoids, whereas the southern part received highly weathered source materials from Archaean K-rich

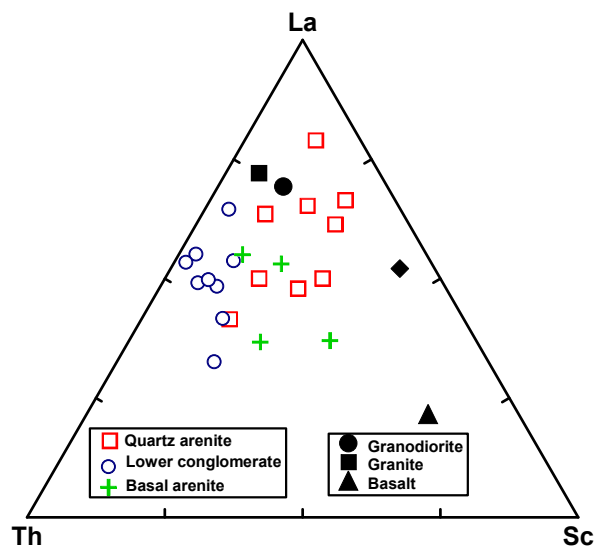
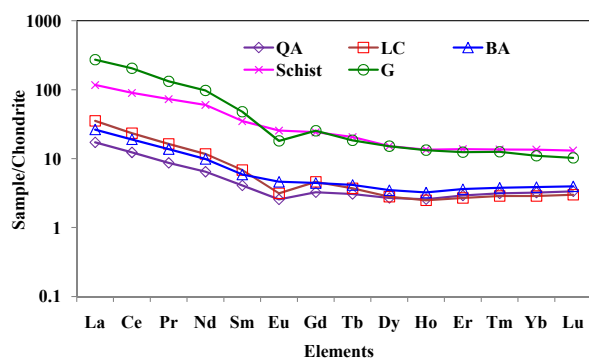


Figure 12. La-Th-Sc diagram. The values of granite, granodiorite, and basalt after Condie (1993).

**Table 5.** Range of elemental ratios of the Kerur Formation compared to the ratios in similar fractions derived from felsic rocks, mafic rocks, and upper continental crust.

Elemental ratio	Range of sandstones from Kerur Formation <sup>1</sup>	Range of sediment from felsic sources <sup>2</sup>	Range of sediment from mafic sources <sup>2</sup>	Upper continental crust (UCC) <sup>3</sup>
Eu/Eu*	0.38–1.13	0.40–0.94	0.71–0.95	0.63
(La/Lu) <sub>cn</sub>	2.66–19.86	3.00–27.0	1.10–7.0	9.73
La/Sc	1.02–25.66	2.50–16.3	0.43–0.86	2.21
Th/Sc	0.25–21.37	0.84–20.5	0.05–0.22	0.79
La/Co	0.06–26.66	1.80–13.8	0.14–0.38	1.76
Th/Co	0.04–11.78	0.67–19.4	0.04–1.10	0.63
Cr/Th	0.67–24.88	4.0–15.0	25–500	7.76

<sup>1</sup>This study.<sup>2</sup>Cullers, 1994b, 2000; Cullers and Podkovyrov, 2000; Cullers et al., 1988.<sup>3</sup>Taylor and McLennan, 1985; McLennan, 2001.**Figure 13.** REE patterns of the present study compared with the granitoids from the Dharwar Craton and basement schist from the Kaladgi-Badami Basin to find out the source rocks of the Kerur Formation (G: granitoids, Jayananda et al., 2000).

granitoids, TTG gneisses, and greenstones (Dey et al., 2009). As a result, REE patterns of the present study are compared with Dharwar Craton granitoids (an average of 11 granites and granodiorites samples; Jayananda et al., 2000) and basement schist from the Kaladgi-Badami Basin to find out the source rocks (Figure 13). Dharwar Craton granitoids show a higher concentration of  $\Sigma$ REE content than the Kerur Formation sedimentary rocks, which is mainly due to their quartzose nature and high  $\text{SiO}_2$  concentration; however, the shape of the REE patterns and the size of the Eu anomaly of the Kerur Formation are similar to Dharwar Craton granitoids and Kaladgi-Badami Basin schist, suggesting that the Archaean Dharwar Craton and basement schist contributed sediments to the Kerur Formation.

## 6. Conclusion

The percentage of  $\text{SiO}_2$  is higher in quartz arenite (87.2%–98.1%) than in lower conglomerate (79.8%–95.9%) and basal arenite (53.5%–90.5%). The  $\text{K}_2\text{O}/\text{Al}_2\text{O}_3$  ratio varies significantly between basal arenite ( $0.61 \pm 0.33$ ), lower conglomerate ( $0.70 \pm 0.11$ ), and quartz arenite ( $0.22 \pm 0.03$ ),

which suggests that basal arenite and lower conglomerate contain considerable amounts of feldspar grains. The REE patterns of the samples studied are LREE-enriched with relatively flat HREE and a negative Eu anomaly. The CIA values of the studied samples suggest that the source region experienced moderate to intense chemical weathering. In the A-CN-K diagram, many samples followed the weathering trend (A-CN line), whereas some followed the A-K trend. The low Cr and Ni contents and high Cr/Ni ratio suggest an absence of ultramafic rocks in the provenance. The REE patterns, trace elemental concentrations, La/Sc versus Th/Co plot, and La-Th-Sc triangular plot suggest that these sediments were mainly derived from felsic rocks. Furthermore, La/Sc, Th/Sc, La/Co, Cr/Th, Eu/Eu\*, and La/Lu ratios compared with sediments derived from felsic and mafic sources also revealed that Proterozoic clastic sediments received sediments mainly from felsic rocks rather than mafic terrains.

## Acknowledgments

The authors thank UGC (No: 41-1032/2012(SR), dt.23.7.2012) and DAE-BRNS for financial support for the project (No. 2008/36/41-BRNS/1969 dated 14/11/2008). They are indebted to the Director, AMD, Hyderabad and Regional Director, Dr AK Rai, AMD, Bangalore for various help. Thanks are also due to Dr Nagaraj, Dr Panneerselvam, Mr Natarajan, Mr Nagendra Kumar, and Dr KT Singh, scientists of AMD-Bangalore, for their help during field work at the Deshnur site. We would like to thank Dr S Kadir and an anonymous reviewer for their critical reviews and constructive comments. Prof Lee thanks the Korea Research Foundation for financial support (grant 2014R1A2A2A01005404 to YIL). We thankfully acknowledge the support and encouragement received from the Professor and Head, Department of Geology, University of Madras. We thank Mr Rufino Lozano-Santa Cruz for his help in XRF analysis. We also thank Mr Pablo Peñaflor Escarcega for powdering of samples for geochemical studies.

## References

- Al-Juboury AI, Al-Hadidy AH (2009). Petrology and depositional evolution of the Palaeozoic rocks of Iraq. *Mar Petrol Geol* 26: 208–231.
- Allen P (1985). The geochemistry of the Amphibolite-Granulite facies transition in Central South India (unpublished Ph.D thesis). New Mexico Institute of Mining and Technology, Socorro, NM, USA.
- Andersson POD, Worden RH, Hodgson DM, Flint S (2004). Provenance evolution and chemostratigraphy of a Palaeozoic submarine fan-complex: Tanqua Karoo Basin, South Africa. *Mar Petrol Geol* 21: 555–577.
- Armstrong-Altrin JS, Lee YI, Verma SP, Ramasamy S (2004). Geochemistry of sandstones from the upper Miocene Kudankulam Formation, southern India: implications for provenance, weathering, and tectonic setting. *J Sediment Res* 74: 285–297.
- Armstrong-Altrin JS, Nagarajan R, Lee YI, Kasper-Zubillaga JJ, Córdoba-Saldaña LP (2014). Geochemistry of sands along the San Nicolas and San Carlos beaches, Gulf of California Mexico: implications for provenance and tectonic setting. *Turkish J Earth Sci* 23: 533–558.
- Armstrong-Altrin JS, Nagarajan R, Madhavaraju J, Rosalez-Hoz L, Lee YI, Balaram V, Cruz-Martinez A, Avila-Ramirez G (2013). Geochemistry of the Jurassic and upper Cretaceous shales from the Molango Region, Hidalgo, Eastern Mexico: Implications of source-area weathering, provenance, and tectonic setting. *CR Geosci* 345: 185–202.
- Bhatia M, Crook KAW (1986). Trace element characteristics of graywackes and tectonic setting discrimination of sedimentary Basin. *Contrib Mineral Pet* 92: 181–193.
- Blatt HG, Middleton GV, Murray RC (1980). *Origin of Sedimentary Rocks*. 2nd ed. Upper Saddle River, NJ, USA: Prentice Hall.
- Colin C, Turpin L, Bertaux J, Desprairies A, Kissel C (1999). Erosional history of the Himalayan and Burman ranges during the last two glacial-interglacial cycles. *Earth Planet Sci Lett* 171: 647–660.
- Concepcion RAB, Dimalanta CB, Yumul GP, Faustino-Eslava DV, Queano KL, Tamayo RA, Imai A (2012). Petrography, geochemistry, and tectonics of a rifted fragment of Mainland Asia: evidence from the Lasala Formation, Mindoro Island, Philippines. *Int J Earth Sci* 101: 273–290.
- Condie KC (1993). Chemical composition and evolution of upper continental crust: Contrasting results from surface samples and shales. *Chem Geol* 104: 1–37.
- Cox R, Lowe DR (1995a). A conceptual review of regional scale controls on the composition of clastic sediment and the co-evolution of continental blocks and their sedimentary cover. *J Sediment Res* 65: 1–12.
- Cox R, Lowe DR (1995b). Compositional evolution of coarse elastic sediments in the south United States from 1.8 to 0.2 G.A. and implications for relationship between the development of crustal blocks and their sedimentary cover. *J Sediment Res* 65: 477–494.
- Cullers RL (1994a). The chemical signature of source rocks in size fraction of Holocene stream sediment derived from metamorphic rocks in the Wet Mountains region, USA. *Chem Geol* 113: 327–343.
- Cullers RL (1994b). The controls on the major and trace element variation of shales, siltstones and sandstones of Pennsylvanian-Permian age from uplifted continental blocks in Colorado to platform sediment in Kansas, USA. *Geochim Cosmochim Acta* 58: 4955–4972.
- Cullers RL (1995). The controls on the major and trace element evolution of shales, siltstones and sandstones of Ordovician to Tertiary age in the Wet Mountain region, Colorado, USA. *Chem Geol* 123: 107–131.
- Cullers RL (2000). The geochemistry of shales, siltstones and sandstones of Pennsylvanian-Permian age, Colorado, U.S.A.: implications for provenance and metamorphic studies. *Lithos* 51: 181–203.
- Cullers RL (2002). Implications of elemental concentrations for provenance, redox conditions, and metamorphic studies of shales and limestones near Pueblo, CO, USA. *Chem Geol* 191: 305–327.
- Cullers RL, Basu A, Suttner LJ (1988). Geochemical signature of provenance in sand-size material in soils and stream sediments near the Tobacco Root batholith, Montana, USA. *Chem Geol* 70: 335–348.
- Cullers RL, Berendsen P (1998). The provenance and chemical variation of sandstones associated with the mid-continent rift system, USA. *Eur J Mineral* 10: 987–1002.
- Cullers RL, Chaudhuri S, Arnold B, Lee M, Wolf CW (1975). Rare-earth distributions in clay minerals and clay-sized fractions of Lower Permian Havensville and Eskridge shales of Kansas and Oklahoma. *Geochim Cosmochim Acta* 39: 1691–1703.
- Cullers RL, Podkovyrov VN (2000). Geochemistry of the Mesoproterozoic Lakhanda shales in southeastern Yakutia, Russia: implications for mineralogical and provenance control, and recycling. *Precamb Res* 104: 77–93.
- Cullers RL, Stone J (1991). Chemical and mineralogical comparison of the Pennsylvanian Mountain, Colorado, U.S.A. (an uplifted continental block) to sedimentary rocks from other tectonic environments. *Lithos* 27: 115–131.
- Degens ET (1965). *Geochemistry of Sediments*. Upper Saddle River, NJ, USA: Prentice Hall.
- Descourvieres C, Douglas G, Leyland L, Hartog N, Prommer H (2011). Geochemical reconstruction of the provenance, weathering and deposition of detrital-dominated sediments in the Perth Basin: the Cretaceous Leederville Formation, south-west Australia. *Sediment Geol* 236: 62–76.
- Dostal J, Keppie JD (2009). Geochemistry of low-grade clastic rocks in the Acatlan Complex of southern Mexico: evidence for local provenance in felsic-intermediate igneous rocks. *Sediment Geol* 222: 241–253.



- Eggins SM, Woodhead JD, Kinsley LPJ, Mortimer GE, Sylvester P, McCulloch MT, Hergt JM, Handler MR (1997). A simple method for the precise determination of  $\geq 40$  trace elements in geological samples by ICPMS using enriched isotope internal standardization. *Chem Geol* 134: 311–326.
- Eriksson KA, Taylor SR, Korsch RJ (1992). Geochemistry of 1.8–1.67 Ga mudstones and siltstones from the Mount Isa Inlier, Queensland, Australia: provenance and tectonic implications. *Geochim Cosmochim Acta* 56: 899–909.
- Ernst W (1970). *Geochemical Facies Analysis*. Amsterdam, the Netherlands: Elsevier.
- Fedo CM, Eriksson KA, Krogstad EG (1996). Stratigraphic framework of the ~3.0 Ga Buhwa greenstone belt: a unique stable shelf succession in the Zimbabwe Archean craton. *Precamb Res* 77: 161–178.
- Fedo CM, Nesbitt HW, Young GM (1995). Unraveling the effects of potassium metasomatism in sedimentary rocks and paleosols, with implications for paleoweathering conditions and provenance. *Geology* 23: 921–924.
- Floyd PA, Shail R, Leveridge BE, Franke W (1991). Geochemistry and provenance of Rhenohercynian synorogenic sandstones: implications for tectonic environment discrimination. *Geol Soc Spec Publ* 57: 173–188.
- Fralic PW, Kronberg BL (1997). Geochemical discrimination of clastic sedimentary rock sources. *Sediment Geol* 113: 111–124.
- Garcia D, Fontelles M, Moutte J (1994). Sedimentary fractionations between Al, Ti, and Zr, and the genesis of strongly peraluminous granites. *J Geol* 102: 411–422.
- Garver JL, Royce PR, Smick TA (1996). Chromium and nickel in shale of the Taconic Foreland: a case study for the provenance of fine-grained sediments with an ultramafic source. *J Sediment Res* 66: 100–106.
- Govindaraju K (1994). Compilation of working values and sample description for 383 standard reference materials. *Geostand Newslett* 18: 331.
- Göz E, Kadir S, Gürel A, Ern M (2014). Geology, mineralogy, geochemistry, and depositional environment of a Late Miocene/Pliocene fluviolacustrine succession, Cappadocian Volcanic Province, central Anatolia, Turkey. *Turkish J Earth Sci* 23: 386–411.
- Gromet LP, Dymek RF, Haskin LA, Korotev RL (1984). The North American shale composite: its compilation, major and trace element characteristics. *Geochim Cosmochim Acta* 48: 2469–2482.
- Grout FF (1925). Relation of texture and composition of clays. *Geol Soc Amer Bull* 36: 393–416.
- Gupta S, Banerjee R, Babu PVR, Parihar PS, Maithani PB (2012). Geochemistry of uraniumiferous Banganapalle sediments in the western part of Palnad Sub-basin, Andhra Pradesh: implications on provenance and paleo-weathering. *Gondwana Geol Mag Spec* 13: 1–14.
- Gürel A, Kadir S (2010). Palaeoenvironmental approach to the geology, mineralogy and geochemistry of an Early Miocene alluvial-fan to cyclic shallow-lacustrine depositional system in the Aktoprak Basin (central Anatolia), Turkey. *Clay Min* 45: 51–75.
- Harnois L (1988). The CIW index: a new chemical index of weathering. *Sediment Geol* 55: 319–322.
- Haskin LA, Wildman RT, Frey FA, Collins KA, Keedy CR, Haskin MA (1966). Rare earths in sediments. *J Geophys Res* 71: 6091–6105.
- Hayashi KI, Fujisawa H, Holland HD, Ohmoto H (1997). Geochemistry of ~1.9 Ga sedimentary rocks from Northeastern Labrador, Canada. *Geochim Cosmochim Acta* 61: 4115–4137.
- Herron MM (1988). Geochemical classification of terrigenous sands and shales from core or log data. *J Sediment Pet* 58: 820–829.
- Hiscott RN (1984). Ophiolitic source rocks for Taconic-age flysch: trace element evidence. *Geol Soc Am* 95: 1261–1267.
- Jacobson AD, Blum JD, Chamberlain CP, Craw D, Koons PO (2003). Climate and tectonic controls on chemical weathering in the New Zealand Southern Alps. *Geochim Cosmochim Acta* 37: 29–46.
- Jayananda M, Moyen JF, Martin H, Peucat JJ, Auvray B, Mahabaleswar B (2000). Late Archaean (2550–2520 Ma) juvenile magmatism in the Eastern Dharwar craton, Southern India: constraints from geochronology, Nd-Sr isotopes and whole rock geochemistry. *Precamb Res* 99: 225–254.
- Jayaprakash AV, Sundaram V, Hans SK, Mishra RN (1987). Geology of the Kaladgi-Badami Basin. *Purana Basins of Peninsular India (Middle to Late Proterozoic)*. *Mem Geol Soc India* 6: 201–226.
- Johnsson MJ (1988). First-cycle quartz arenites in the Orinoco river basin, Venezuela and Colombia. *J Geol* 96: 263–277.
- Jung HS, Lim D, Choi JC, Yoo HS, Rho KC, Lee HB (2012). Rare earth element compositions of core sediments from the shelf of the south Sea, Korea: their controls and origins. *Cont Shelf Res* 48: 75–86.
- Kadir S, Gürel A, KÜlah T (2013). Geology of Late Miocene clayey sediments and distribution of palaeosol clay minerals in the north-eastern part of the Cappadocian Volcanic Province (Araph-Erdemli), central Anatolia, Turkey. *Turkish J Earth Sci* 22: 427–443.
- KÜlah T, Kadir S, Gürel A, Eren M, Önalgil N (2014). Mineralogy, geochemistry and genesis of mudstones in the Upper Miocene Mustafapaşa member of the Ürgüp Formation in the Cappadocia region, central Anatolia, Turkey. *Clays Clay Min* 62: 267–285.
- Madhavaraju J (2015). Geochemistry of Late Cretaceous sedimentary rocks of the Cauvery Basin, South India: constraints on paleoweathering, provenance and end Cretaceous environments. In: Ramkumar, M, editor. *Chemostratigraphy: Concepts, Techniques and Applications*. 1st ed. Elsevier, the Netherlands, pp. 185–214.
- Madhavaraju J, González-León CM (2012). Depositional conditions and source of rare earth elements in carbonate strata of the Aptian-Albian Mural Formation, Pitaycachi section, northeastern Sonora, Mexico. *Rev Mex Cien Geol* 29: 478–491.
- Madhavaraju J, González-León CM, Lee YI, Armstrong-Altrin JS, Reyes Campero LM (2010). Geochemistry of the Mural Formation (Aptian-Albian) of the Bisbee Group, Northern Sonora, Mexico. *Cre Res* 31: 400–414.

- Madhavaraju J, Lee YI (2010). Influence of Deccan volcanism in the sedimentary rocks of Late Maastrichtian-Danian age of Cauvery basin Southeastern India: constraints from geochemistry. *Current Sci* 98: 528–537.
- Madhavaraju J, Lee YI (2009). Geochemistry of the Dalmiapuram Formation of the Uttatur Group (Early Cretaceous), Cauvery basin, southeastern India: implications on provenance and paleo-redox conditions. *Rev Mex Cien Geol* 26: 380–394.
- Madhavaraju J, Löser H, Lee YI, Lozano Santacruz R, Pi-Puig T (2015). Geochemistry of Lower Cretaceous limestones of the Alisitos Formation, Baja California, México: implications for REE source and paleo-redox conditions. *J South Amer Earth Sci* (in press).
- Madhavaraju J, Ramasamy S (2001). Clay mineral assemblages and rare earth element distribution in the sediments of Ariyalur Group, Tiruchirapalli District, Tamil Nadu- Implication for paleoclimate. *J Geol Soc India* 58: 69–77.
- Madhavaraju J, Ramasamy S (2002). Petrography and geochemistry of Late Maastrichtian-Early Paleocene sediments of Tiruchirapalli Cretaceous, Tamil Nadu – Paleoweathering and provenance implications. *J Geol Soc India* 59: 133–142.
- Madhavaraju J, Ramasamy S, Mohan SP, Hussain SM, Gladwin Gnana Asir N, Stephen Pitchaimani V (2004). Petrography and surface textures on quartz grains of Nimar Sandstone, Bagh Beds, Madhya Pradesh - implications on provenance and depositional environments. *J Geol Soc India* 64: 747–762.
- Maynard JB, Valloni R, Yu H (1982). Composition of modern deep sea sands from arc-related basins. *Geol Soc Spec Publ* 10: 551–561.
- McCulloch MT, Wasserburg GJ (1978). Sm-Nd and Rb-Sr chronology of continental crust formation. *Science* 200: 1003–1011.
- McLennan SM (1989). Rare earth elements in sedimentary rocks: influences of provenance and sedimentary processes. In: Lipin BR, McKay GA, editors. *Geochemistry and Mineralogy of Rare Earth Elements*. Reviews in Mineralogy, Vol. 21. Chantilly, VA, USA: Mineralogical Society of America, pp. 169–200.
- McLennan SM (2001). Relationships between the trace element composition of sedimentary rocks and upper continental crust. *Geochem Geophys Geosyst* 2: 2000GC000109.
- McLennan SM, Bock B, Hemming SR, Hurowitz JA, Lev SM, McDaniel DK (2004). The roles of provenance and sedimentary processes in the geochemistry of sedimentary rocks. In: Lentz DR, editors. *Geochemistry of Sediments and Sedimentary Rocks: Evolutionary Considerations to Mineral Deposit-Forming Environments*. St. John's, NL, Canada: Geological Association of Canada, GeoText.
- McLennan SM, Hemming S, McDaniel DK, Hanson GN (1993). Geochemical approaches to sedimentation, provenance and tectonics. In: Johnsson MJ, Basu A, editors. *Processes Controlling the Composition of Clastic Sediments*. Special Paper 284. Boulder, CO, USA: Geological Society of America, pp. 21–40.
- McLennan SM, Taylor SR (1982). Geochemical constraints on the growth of the continental crust. *J Geol* 90: 347–361.
- McLennan SM, Taylor SR (1991). Sedimentary rocks and crustal evolution: tectonic setting and secular trends. *J Geol* 99: 1–21.
- McLennan SM, Taylor SR, Eriksson KA (1983). Geochemistry of Archaean shales from the Pilbara Supergroup, Western Australia. *Geochim Cosmochim Acta* 47: 1211–1222.
- McLennan SM, Taylor SR, McCulloch MT, Maynard JB (1990). Geochemical and Nd-Sr isotopic composition of deep-sea turbidites: crustal evolution and plate tectonic associations. *Geochim Cosmochim Acta* 54: 2015–2050.
- Mishra M, Sen S (2012). Provenance, tectonic setting and source-area weathering of Mesoproterozoic Kaimur Group, Vindhyan Supergroup, Central India. *Geol Acta* 10: 283–293.
- Moosavirad SM, Janardhana MR, Sethumadhav MS, Narasimha KNP (2012). Geochemistry of Lower Jurassic sandstones of Shemshak Formation, Kerman Basin, Central Iran: provenance, source weathering and tectonic setting. *J Geol Soc India* 79: 483–496.
- Nagarajan R, Armstrong-Altrin JS, Nagendra R, Madhavaraju J, Moutte J (2007a). Petrography and geochemistry of terrigenous sedimentary rocks in the Neoproterozoic Rabanpalli Formation, Bhima Basin, southern India: implications for paleoweathering condition, provenance, and source rock composition. *J Geol Soc India* 70: 297–312.
- Nagarajan R, Madhavaraju J, Armstrong-Altrin JS, Nagendra R (2011). Geochemistry of Neoproterozoic limestones of the Shahabad Formation, Bhima Basin, Karnataka, southern India. *Geosci J* 15: 9–25.
- Nagarajan R, Madhavaraju J, Nagendra R, Armstrong-Altrin JS, Moutte J (2007b). Geochemistry of Neoproterozoic shales of Rabanpalli Formation, Bhima Basin, Northern Karnataka, Southern India: implications for provenance and paleoredox conditions. *Rev Mex Cien Geol* 24: 150–160.
- Nesbitt HW, Fedo CM, Young GM (1997). Quartz and feldspar stability, steady and non-steady-state weathering and petrogenesis of siliciclastic sands and muds. *J Geol* 105: 173–191.
- Nesbitt HW, Markovics G, Price RC (1980). Chemical processes affecting alkalis and alkaline earths during continental weathering. *Geochim Cosmochim Acta* 44: 1659–1666.
- Nesbitt HW, Young GM (1982). Early Proterozoic climates and plate motions inferred from major element chemistry of lutites. *Nature* 299: 715–717.
- Nesbitt HW, Young GM (1984). Prediction of some weathering trends of plutonic and volcanic rocks based on thermodynamic and kinetic considerations. *Geochim Cosmochim Acta* 48: 1523–1534.
- Perri F, Critelli S, Mongelli G, Cullers RL (2011). Sedimentary evolution of the Mesozoic continental redbeds using geochemical and mineralogical tools: the case of Upper Triassic to Lowermost Jurassic Monte di Gioiosa mudrocks (Sicily, southern Italy). *Int J Earth Sci* 100: 1569–1587.
- Ramasamy S, Singh TS, Madhavaraju J, Gladwin Gnana Asir N (2007). Petrography and geochemistry of pre-Ariyalur sequence in Ariyalur District, Tamil Nadu-implication on depositional environment and paleoclimate. *J Geol Soc India* 69: 121–132.

- Raza M, Ahmad AHM, Khan MS, Khan F (2012). Geochemistry and detrital modes of Proterozoic sedimentary rocks, Bayana Basin, north Delhi fold belt: implications for provenance and source-area weathering. *Int Geol Rev* 54: 1 111–129.
- Roser BP, Cooper RA, Nathan S, Tulloch AJ (1996). Reconnaissance sandstone geochemistry, provenance, and tectonic setting of the lower Paleozoic terranes of the West Coast and Nelson, New Zealand. *NZ J Geol Geophys* 39: 1–16.
- Roser BP, Korsch RJ (1986). Determination of tectonic setting of sandstone-mudstone suites using SiO<sub>2</sub> content and K<sub>2</sub>O/Na<sub>2</sub>O ratio. *J Geol* 94: 635–650.
- Roser BP, Korsch RJ (1988). Provenance signatures of sandstone-mudstone suites determined using discrimination function analysis of major-element data. *Chem Geol* 67: 119–139.
- Sawyer EW (1986). The influence of source rock type, chemical weathering and sorting on the geochemistry of clastic sediments from the Quetico metasedimentary belt, Superior Province, Canada. *Chem Geol* 55: 77–95.
- Schoenborn WA, Fedo CM (2011). Provenance and paleoweathering reconstruction of the Neoproterozoic Johnnie Formation, southeastern California. *Chem Geol* 285: 231–255.
- Selvaraj K, Chen CTA (2006). Moderate chemical weathering of subtropical Taiwan: constraints from solid-phase geochemistry of sediments and sedimentary rocks. *J Geol* 14: 101–116.
- Shadan M, Hosseini-Barzi M (2013). Petrography and geochemistry of the Ab-e-Haji Formation in central Iran: implications for provenance and tectonic setting in the southern part of the Tabas block. *Rev Mex Cien Geol* 30: 80–95.
- Singh P (2009). Major, trace and REE geochemistry of the Ganga River sediments: influence of provenance and sedimentary processes. *Chem Geol* 266: 242–255.
- Srivastava AK, Randive KR, Khare N (2013). Mineralogical and geochemical studies of glacial sediments from Schirmacher Oasis, East Antarctica. *Quatern Int* 292: 205–216.
- Suttner LJ, Dutta PK (1986). Alluvial sandstone composition and paleoclimate frame work mineralogy. *J Sediment Pet* 56: 329–345.
- Taylor SR, McLennan SM (1985). *The Continental Crust: Its Composition and Evolution*. Oxford, UK: Blackwell.
- Verma SP, Armstrong-Altrin JS (2013). New multi-dimensional diagrams for tectonic discrimination of siliciclastic sediments and their application to Precambrian basins. *Chem Geol* 355: 117–133.
- Wronkiewicz DJ, Condie KC (1987). Geochemistry of Archaean shales from the Witwatersrand Supergroup, South Africa. Source-area weathering and provenance. *Geochim Cosmochim Acta* 51: 2401–2416.
- Wronkiewicz DJ, Condie KC (1989). Geochemistry and provenance of sediments from the Pongola Supergroup, South Africa: evidence for a 3.0 Ga old continental craton. *Geochim Cosmochim Acta* 53: 537–549.
- Wronkiewicz DJ, Condie KC (1990). Geochemistry and mineralogy of sediments from the Ventersdorp and Transvaal Supergroups, South Africa. Cratonic evolution during the early Proterozoic. *Geochim Cosmochim Acta* 54: 343–354.
- Wu W, Zheng H, Xu S, Yang J, Liu W (2013). Trace element geochemistry of riverbed and suspended sediments in the upper Yangtze River. *J Geochem Explor* 124: 67–78.
- Young SM, Pitawala A, Ishiga H (2013). Geochemical characteristics of stream sediments, sediment fractions, soils, and basement rocks from the Mahaweli River and its catchment, Sri Lanka. *Chem Erde Geochem* 73: 357–371.
- Zaid SM, Elbadry O, Ramadan F, Mohamed M (2015). Petrography and geochemistry of Pharaonic sandstone monuments in Tall San Al Hagr, Al Sharqiya Governorate, Egypt: implications for provenance and tectonic setting. *Turkish J Earth Sci* 24: 344–364.
- Zaid SM, Gahtani FA (2015). Provenance, diagenesis, tectonic setting, and geochemistry of Hawkesbury Sandstone (Middle Triassic), southern Sydney Basin, Australia. *Turkish J Earth Sci* 24: 72–98.
- Zhang YL, Wang ZQ, Yan Z, Wan T (2011). Tectonic setting of Neoproterozoic Beiyixi Formation in Quruqtagh area, Xinjiang: evidence from geochemistry of clastic rocks. *Acta Petrol Sin* 27: 1785–1796.